

Real-World Single Image Super-Resolution: A Brief Review

Honggang Chen, Xiaohai He, Linbo Qing, Yuanyuan Wu, Chao Ren, and Ce Zhu

Abstract—Single image super-resolution (SISR), which aims to reconstruct a high-resolution (HR) image from a low-resolution (LR) observation, has been an active research topic in the area of image processing in recent decades. Particularly, deep learning-based super-resolution (SR) approaches have drawn much attention and have greatly improved the reconstruction performance on synthetic data. Recent studies show that simulation results on synthetic data usually overestimate the capacity to super-resolve real-world images. In this context, more and more researchers devote themselves to develop SR approaches for realistic images. This article aims to make a comprehensive review on real-world single image super-resolution (RSISR). More specifically, this review covers the critical publically available datasets and assessment metrics for RSISR, and four major categories of RSISR methods, namely the degradation modeling-based RSISR, image pairs-based RSISR, domain translation-based RSISR, and self-learning-based RSISR. Comparisons are also made among representative RSISR methods on benchmark datasets, in terms of both reconstruction quality and computational efficiency. Besides, we discuss challenges and promising research topics on RSISR.

Index Terms—Super-resolution, Real-world image, Deep learning, Datasets, Assessment Metrics, Review

I. INTRODUCTION

HIGH-RESOLUTION (HR) images are desired urgently in many application areas such as intelligent surveillance, medical imaging, and remote sensing. To obtain images with higher resolution, a natural idea is to upgrade the hardware (*e.g.*, the imaging system). Although recent years have witnessed the obvious progress of imaging devices and techniques, this kind of approach has two main limitations: (i) It is inflexible and costly because the demand in practical applications is constantly changing. (ii) It can be used only for capturing new HR images, but not for enhancing the resolution of existing low-resolution (LR) images. Compared to the hardware upgrade-based “hard” solution, the signal processing-based “soft” image resolution enhancement known as super-resolution (SR) is more flexible and economical. With the SR techniques that reconstruct a

This work was supported by the National Natural Science Foundation of China under Grant 62001316, Grant 61801316, and Grant 61871279. (*Corresponding author: Chao Ren.*)

Honggang Chen, Xiaohai He, Linbo Qing, and Chao Ren are with the College of Electronics and Information Engineering, Sichuan University, Chengdu 610065, China (e-mail: honggang_chen@scu.edu.cn; hxx@scu.edu.cn; qing_lb@scu.edu.cn; chaoren@scu.edu.cn).

Yuanyuan Wu is with the College of Information Science and Technology, Chengdu University of Technology, Chengdu, China, 610059 (e-mail: wuyuan@cdut.edu.cn).

Ce Zhu is with the School of Information and Communication Engineering, University of Electronic Science and Technology of China, Chengdu 611731, China (e-mail: eczhu@uestc.edu.cn)

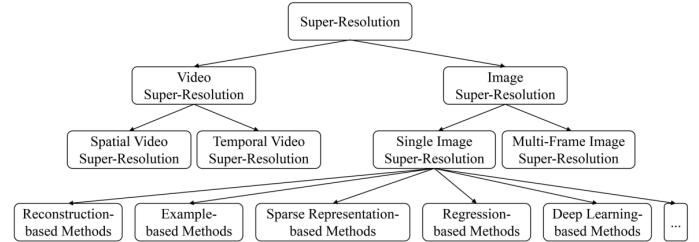


Fig. 1. The taxonomy of existing super-resolution techniques.

higher resolution output from the LR observation, we can obtain images with the resolution beyond the limit of imaging systems, thereby benefiting the subsequent analysis and understanding tasks such as segmentation [1]–[4], detection [5]–[7], and recognition [8]–[10].

In general, as presented in Fig. 1, existing SR techniques can be grouped into two categories according to the LR input and the reconstructed HR output, *i.e.*, video super-resolution (VSR) [11]–[27] and image super-resolution (ISR) [28]–[78]. On the whole, VSR aims to improve the spatial resolution (known as spatial VSR) [11]–[19] or the frame rate (known as temporal VSR) [20]–[27] of the observed video. ISR can be further classified into multi-frame image super-resolution (MISR) [28]–[35] and single image super-resolution (SISR) [36]–[78]. MISR refers to reconstructing an HR image via fusing the complementary information in a series of correlated images of the same scene [28]–[35], while SISR generates an HR image from one LR observation [36]–[78]. In terms of application scenarios, SISR is more practical than MISR and VSR because it is much less demanding on the input, which is one reason why SISR attracts wider attention. A variety of SISR methods have been proposed in the past decades, mainly including reconstruction-based [36]–[45], example-based [46]–[52], sparse representation-based [53]–[60], regression-based [61]–[66], and deep learning-based approaches [67]–[78], *etc.* Particularly, the deep learning-based SISR methods [67]–[78] developed in recent years take the SR performance on synthetic LR images (*e.g.*, bicubically downsampled images) to a new level.

Nevertheless, previous research [79] shows that the actual SR ability of most existing SISR methods may be overestimated based only on synthetic data due to the domain gap between synthetic and realistic data. In other words, compared to the promising SR results on synthetic test images, the SR performance would degrade significantly on real-world images, thus hindering the practical applications of SISR

algorithms. To address this problem, some researchers have shifted their focus to real-world single image SR (RSISR) over the past couple of years, and a series of studies involving real-world dataset collection [79]–[87], SR models for real-world images [79]–[115], and SR result assessment [116]–[119] have been conducted. Meanwhile, several challenges on RSISR have been organized in conjunction with the *IEEE Conference on Computer Vision and Pattern Recognition (CVPR)*, *IEEE International Conference on Computer Vision (ICCV)*, and *European Conference on Computer Vision (ECCV)* to attract more attention and promote the development of RSISR techniques [120]–[123]. It is exciting to see that the studies on RSISR are becoming more targeted and the SR performance on real-world images is improved increasingly.

In this work, we mainly give an overview of recent RSISR algorithms and relevant studies. There are several works concerning the overview of image and video SR techniques. For example, Yue *et al.* [124] make a summary of the techniques, applications and future of image SR. Considering that deep learning has been widely employed to address SR over the past few years, more recently Yang *et al.* [125], Wang *et al.* [126], and Liu *et al.* [127] review deep learning-based image/video SR methods. However, this work is the first attempt to make an overview of RSISR techniques to the best of our knowledge. The main contributions of this review are four-fold: (i) We comprehensively review the studies on RSISR, including datasets, assessment metrics, technologies and methods, *etc.* (ii) We present a taxonomy for existing RSISR methods according to their primary principles. (iii) We compare the reconstruction accuracy and efficiency of representative RSISR algorithms on benchmark datasets. (iv) We further discuss current challenges and future research directions for RSISR.

The rest of this review is organized as follows. The background of RSISR is briefly introduced in Section II. In Section III, the datasets and assessment metrics for RSISR are described. Section IV reviews RSISR technologies and methods by category. The comparisons among representative RSISR algorithms are presented in Section V. In Section VI, we analyze current challenges and future research directions of RSISR. Finally, Section VII concludes this work.

II. BACKGROUND

SISR refers to reconstructing an HR image from an LR observation. Given an LR image \mathbf{Y} , it is generally assumed to be degraded from a corresponding HR image \mathbf{X} , which can be represented as

$$\mathbf{Y} = D(\mathbf{X}, \theta_D) \quad (1)$$

where $D(\cdot)$ denotes the degradation process defined by the parameter set θ_D . Note that in a real scenario, the degradation parameter θ_D is unknown, and all we have is the LR image \mathbf{Y} . SISR aims at recovering a good estimate of the potential HR image via reversing the degradation process shown in Eq. (1), which can be formulated as

$$\hat{\mathbf{X}} = R(\mathbf{Y}, \theta_R) \quad (2)$$

where $R(\cdot)$ represents the SR function and θ_R is the corresponding parameter set. $\hat{\mathbf{X}}$ is the super-resolved image from \mathbf{Y} , *i.e.*, an estimate of the real HR image \mathbf{X} .

Apparently, the SR process and degradation process are the inverses of each other. Thus, for obtaining excellent reconstruction performance, the SR function $R(\mathbf{Y}, \theta_R)$ should be adapted to the degradation $D(\mathbf{X}, \theta_D)$. In the literature, some researchers [36]–[45] approximate the degradation via blurring, downsampling, and noise injection. Mathematically, the simulated degradation process is as follows

$$\mathbf{Y} = \mathbf{SBX} + \mathbf{n} \quad (3)$$

where \mathbf{B} and \mathbf{S} denote the operations of blurring and downsampling, respectively. In general, the blurring is realized via convolving the HR image with a Gaussian kernel. \mathbf{n} represents the additive noise, which is usually assumed to be white Gaussian noise. Part of works [61]–[78] adopt a simpler degradation model, *i.e.*, directly downscaling an HR image using the “bicubic” kernel to generate corresponding LR image. For comparison and evaluation, most existing SR methods are developed and validated on synthetic LR images generated by degradation simulations. Overall, the SR reconstruction performance on synthetic LR images is rather good, especially for deep learning-based SISR approaches such as RCAN [73], SAN [75], and RFANet [77].

Compared with the commonly used degradation model in simulations, the actual degradation in real-world scenarios is more complex and varying because it can be affected by a number of factors (*e.g.*, imaging system and imaging environment). In other words, the degradation model used in simulations may not match that suffered by real-world images, which results in the domain gap between synthetic LR images and realistic LR observations. For this primary reason, the reconstruction performance of most existing SISR algorithms drops significantly on real-world images. To enhance quality of super-resolving real-world images, some researchers have been working on RSISR from different perspectives in the past several years, including realistic dataset building, SR model development, SR performance assessment, *etc.*

III. DATASETS AND ASSESSMENT METRICS

Training/testing datasets and assessment metrics are the cornerstones of the SISR. In this section, we briefly introduce the relevant datasets and assessment metrics.

A. Datasets for RSISR

For the training and testing of SISR models, the widely used datasets include DIV2K [128], BSDS500 [129], T91 [53], Set5 [130], Set14 [54], Urban100 [50], Manga109 [131], *etc.* Most of these datasets only contain HR images. In this case, we need to generate LR counterparts based on the assumed degradation model (*e.g.*, “bicubic” kernel-based downsampling), both for model training and testing. Therefore, these datasets are not quite suitable for the study of RSISR due to the significant discrepancy between the assumed degradation model and the real one. To address this problem, some more targeted datasets for RSISR have been constructed

TABLE I
AN OVERVIEW OF DATASETS FOR RSISR.

Datasets	Published	Synthetic / Realistic	Scale Factors	Keywords
DIV2K _{RR}	NeurIPS-2019 [94]	Synthetic	$\times 2, \times 4$	DIV2K, Random kernels, Uniform multiplicative noise
RealSR	ICCV-2019 [80]	Realistic	$\times 2, \times 3, \times 4$	Focal length adjusting
DRealSR	ECCV-2020 [81]	Realistic	$\times 2, \times 3, \times 4$	Focal length adjusting
City100	CVPR-2019 [82]	Realistic	$\times 2.9, \times 2.4$	Focal length adjusting, Shooting distance changing
SR-RAW	CVPR-2019 [83]	Realistic	$\times 4, \times 8$	Focal length adjusting, RAW data
TextZoom	ECCV-2020 [84]	Realistic	$\times 2$	Text, Recognition
SupER	TPAMI-2020 [79]	Realistic	$\times 2, \times 3, \times 4$	Hardware binning, Image sequences
ImagePairs	CVPRW-2020 [85]	Realistic	$\times 2$	Beam-splitter cube, RAW data

in different ways, including DIV2K_{RR} [94], RealSR [80], DRealSR [81], City100 [82], SR-RAW [83], TextZoom [84], SupER [79], ImagePairs [85], *etc.* Table I summarizes the above datasets.

1) *DIV2K_{RR}* [94]: This is a synthetic testing dataset built by Bell-Kligler *et al.* [94] for blind SR.¹ The DIV2K_{RR} [94] is derived from DIV2K [128] that contains diverse 2K resolution images. DIV2K is proposed by Agustsson *et al.* [128] for NTIRE 2017 SR challenge. More specifically, the 100 HR images in the validation set of DIV2K [128] are blurred and downsampled with random kernels to generate LR counterparts. Random blur kernels are 11×11 anisotropic gaussians, and each of them is with two independently distributed lengths $\lambda_1, \lambda_2 \sim u(0.6, 5)$ and a rotation angle $\theta \sim u[-\pi, \pi]$. Further, uniform multiplicative noise is applied to the blur kernel before normalizing its sum to one. DIV2K_{RR} [94] is still a synthetic dataset, although the degradation model is more complex and random.

2) *RealSR* [80]: RealSR is a real-world dataset collected by Cai *et al.* [80] for training and testing RSISR models.² RealSR consists of 595 LR-HR image pairs obtained by adjusting the lens of two digital single lens reflex (DSLR) cameras (*i.e.*, Nikon D810 and Canon 5D3). To study the RSISR with different scaling factors (*e.g.*, $\times 2, \times 3, \times 4$), images are taken at four focal lengths, *i.e.*, 28mm, 35mm, 50mm, and 105mm. Naturally, for the same scene, the images captured at 105mm are used as HR images, and the images captured at 28mm, 35mm, and 50mm are seen as LR counterparts for $\times 4, \times 3$, and $\times 2$ upsampling, respectively. Considering the differences (*e.g.*, lens distortion and exposures) among the images captured at different focal lengths, Cai *et al.* [80] further propose a progressive image registration framework to achieve pixel-wise registration of images taken at 28mm, 35mm, 50mm, and 105mm. First, PhotoShop is used to correct the lens distortion and the regions of interest around the center of the corrected images are cropped. Then, the regions cropped

from the images captured at 105mm are used as HR references, and the corresponding regions cropped from the images taken at 28mm, 35mm, and 50mm are aligned to generate LR counterparts via iteratively optimizing the parameters of affine transformation and luminance adjustment. After convergence, real-world LR-HR image pairs can be obtained.

3) *DRealSR* [81]: The real-world dataset DRealSR built by Wei *et al.* [81] is similar to RealSR [80], with a larger scale.³ More specifically, five DLSR cameras (*i.e.*, Sony, Canon, Olympus, Nikon, and Panasonic) are used to capture images at four resolutions in outdoor and indoor scenes (*e.g.*, buildings, offices, plants, posters, *etc.*). The SIFT algorithm [132] is adopted to align the images with different resolutions. In total, DRealSR [81] contains 884, 783, and 840 LR-HR image pairs for $\times 2, \times 3$, and $\times 4$ SR, respectively.

4) *City100* [82]: The City100 dataset proposed by Chen *et al.* [82] includes City100_NikonD5500 and City100_iPhoneX, which characterize the resolution and field-of-view (FoV) degradation under DSLR and smartphone cameras, respectively.⁴ As is well known, there is a tradeoff between the resolution and FoV for imaging systems. An image with a larger FoV but a lower resolution can be obtained when zooming out the lens, while the image resolution can be enhanced at the expense of a reduced FoV when zooming in the lens. Therefore, Chen *et al.* propose [82] to adjust the focal length or shooting distance to capture images of the same scene with different resolutions. 100 postcards of different city scenes are used as imaging subjects. For the City100_NikonD5500 dataset taken by NikonD5500, HR and LR images are captured at the focal length of 55mm and 18mm, respectively. The HR and LR images of the same scene are first spatially aligned based on SIFT key-points [132] and RANSAC [133]. Further, intensity and color rectification is conducted to improve the accuracy of alignment. The main distinction between City100_iPhoneX and City100_NikonD5500 is that City100_iPhoneX is captured by iPhone X via changing the shooting distance.

5) *SR-RAW* [83]: The SR-RAW dataset proposed by Zhang *et al.* [83] is composed of pairs of RAW images taken at different levels of optical zoom.⁵ The SR-RAW [83] is similar to the RealSR [80] mentioned above in terms of the way to capture images of the same scene with different resolutions, *i.e.*, adjusting the focal length. For SR-RAW [83], seven images of each scene are taken under seven different optical zoom settings using a 24-240mm zoom lens (*i.e.*, Sony FE 24-240mm). In total, 500 seven-image sequences are collected in outdoor and indoor scenes. For image registration, the Euclidean motion model is applied to describe the relationship between the images with different resolutions and it is optimized by minimizing the enhanced correlation coefficient as in [134]. Unlike the RealSR built by Cai *et al.* [80], SR-RAW [83] contains both raw sensor

³DRealSR [81] is available at <https://github.com/xiezw5/Component-Divide-and-Conquer-for-Real-World-Image-Super-Resolution>

⁴City100 [82] is available at <https://github.com/ngchc/CameraSR>

⁵SR-RAW [83] is available at <https://ceciliavision.github.io/project-pages/project-zoom.html>

¹DIV2K_{RR} [94] is available at <http://www.wisdom.weizmann.ac.il/~vision/kernelgan/>

²RealSR [80] is available at <https://github.com/csycjai/RealSR>

data and RGB images because it is used for SR from raw data. That is, instead of the LR RGB image, its raw sensor data is used as the input to reconstruct the corresponding HR RGB image. Actually, the reconstruction process covers demosaicing, denoising, SR, *etc.* Compared with 8-bit RGB images, as pointed out in [83], raw sensor data generally contains more useful information for SR.

6) *TextZoom* [84]: The *TextZoom* derived from *RealSR* [80] and *SR-RAW* [83] is the first real scene text SR dataset constructed by Wang *et al.* [84].⁶ More specifically, the text images in *TextZoom* [84] are cropped from the images in *RealSR* [80] and *SR-RAW* [83], including various natural scenes such as shops, street views, and vehicle interiors. The content, direction, and focal length of each LR-HR text image pair in *TextZoom* are provided in the annotation process. Moreover, *TextZoom* [84] comprises three subsets according to difficulty levels, namely easy, medium, and hard. Thanks to the well-organized annotations, *TextZoom* [84] can be utilized to study text image SR as well as text recognition.

7) *SupER* [79]: The *SupER* is built by Köhler *et al.* [79] via hardware binning.⁷ More specifically, more than 80,000 images are taken from 14 lab scenes at four imaging resolutions and five compression levels, using a Basler acA2000-50gm CMOS camera with a $f/1.8$, 16mm fixed-focus lens. What is special about *SupER* [79] is that the imaging resolution is adjusted by changing the binning factor, which naturally guarantees the perfect alignment between LR and HR images. Three binning factors (*i.e.*, 2, 3, and 4) are used to acquire LR images corresponding to the same HR image at three different resolution levels. Meanwhile, to enhance the comprehensiveness, four motion types, two photometric conditions, and five H.265 compression levels are considered while building *SupER* [79]. Additionally, unlike most existing datasets for SISR, image sequences instead of independent images are captured in *SupER* [79], which is also applicable in the study on MISR algorithms.

8) *ImagePairs* [85]: The *ImagePairs* proposed by Joze *et al.* [85] includes 11,421 LR-HR image pairs of diverse scenes, in which LR and HR images are captured by an LR camera (5MP) and an HR camera (20.1MP), respectively.⁸ More specifically, a beam-splitter cube is used to make the two cameras capture images of the same scene simultaneously. Due to the difference in focal length, the LR and HR cameras have different perspectives. Therefore, Joze *et al.* [85] propose to generate pixel-wise aligned LR-HR image pairs via applying the following four steps: ISP, image undistortion, pair alignment, and margin cropping. The raw data collected by LR and HR cameras are first converted to color images in the ISP process. Then, distortions (*e.g.*, tangential and radial distortions) caused by cameras are reduced via camera calibration. Further, LR and HR images are aligned globally and locally. Finally, 10% of the border is removed from each image to improve the matching accuracy of image pairs. In

TABLE II
AN OVERVIEW OF WIDELY USED ASSESSMENT METRICS FOR RSISR.

Metrics	Published	Full/No-reference	Keywords
PSNR	-	Full-reference	Mean squared error
SSIM	TIP-2004 [135]	Full-reference	Structure similarity, Luminance, Contrast, Structures
IFC	TIP-2005 [136]	Full-reference	Nature scene statistics, Gaussian scale mixtures
LPIPS	CVPR-2018 [137]	Full-reference	Deep features, Human perceptual similarity
NIQE	SPL-2012 [138]	No-reference	Quality-aware features, Multivariate Gaussian model
PIQE	NCC-2015 [139]	No-reference	Perceptually significant spatial regions, Block level distortion map
NRQM	CVIU-2017 [116]	No-reference	Statistical features, Regression forests, Linear regression model

addition to SR, *ImagePairs* [85] may be used for ISP and other tasks as it includes raw images.

B. Assessment Metrics for Super-Resolved Images

In general, the quality assessment of super-resolved images is two-fold, *i.e.*, human perception-based subjective evaluation and quality metrics-based objective evaluation. Overall, the former is a more direct way and it is more in agreement with the practical need. However, subjective evaluation suffers the following limitations. (i) The assessment result is readily affected by personal preferences. (ii) The evaluation process is often costly and cannot be automated. By contrast, objective evaluation is more convenient to use, although the results by different assessment metrics may not be necessarily consistent with each other as well as subjective evaluation. Table II reports commonly used metrics for evaluating the objective quality of super-resolved images, including PSNR, SSIM [135], IFC [136], LPIPS [137], NIQE [138], PIQE [139], and NRQM [116]. For the description, let $\mathbf{X} \in \mathbb{R}^{H \times W \times C}$ and $\hat{\mathbf{X}} \in \mathbb{R}^{H \times W \times C}$ denote the ground truth image and the super-resolved image, respectively. H , W , and C denote width, height, and number of components, respectively.

1) *PSNR*: Peak signal-to-noise ratio (PSNR) is the most widely used full-reference objective quality assessment metric for image restoration (*e.g.*, SR, denoising, deblocking, and deblurring). Given $\hat{\mathbf{X}}$ and \mathbf{X} , the PSNR is defined as

$$\text{PSNR} = 10 \cdot \log_{10} \left(\frac{L^2}{\text{MSE}} \right) \quad (4)$$

where $\text{MSE} = \frac{1}{HWC} \left\| \mathbf{X} - \hat{\mathbf{X}} \right\|_2^2$ denotes the mean squared error (MSE) between $\hat{\mathbf{X}}$ and \mathbf{X} , and L represents the maximum pixel value (*i.e.*, 255 for 8-bit images). It can be seen from Eq. (4) that PSNR is more concerned with the proximity between corresponding pixels in $\hat{\mathbf{X}}$ and \mathbf{X} , which results in the low consistency with perceptual quality in some cases.

2) *SSIM* [135]: The structure similarity index (SSIM) [135] is a full-reference objective quality assessment metric that measures structural similarity.⁹ More specifically, the

⁶*TextZoom* [84] is available at <https://github.com/JasonBoyl/TextZoom>

⁷*SupER* [79] is available at <https://www.lms.tf.fau.eu/research/downloads/superresolution/>

⁸*ImagePairs* [85] is available at www.microsoft.com/en-us/research/project/imagepairs

⁹The source code of SSIM [135] is available at https://live.ece.utexas.edu/research/Quality/index_algorithms.htm

comparisons are jointly performed in the aspects of luminance, contrast, and structures as

$$\text{SSIM} = [l(\mathbf{X}, \hat{\mathbf{X}})]^\alpha [c(\mathbf{X}, \hat{\mathbf{X}})]^\beta [s(\mathbf{X}, \hat{\mathbf{X}})]^\gamma \quad (5)$$

where $l(\mathbf{X}, \hat{\mathbf{X}}) = \frac{2\mu_{\mathbf{X}}\mu_{\hat{\mathbf{X}}} + C_1}{\mu_{\mathbf{X}}^2 + \mu_{\hat{\mathbf{X}}}^2 + C_1}$, $c(\mathbf{X}, \hat{\mathbf{X}}) = \frac{2\sigma_{\mathbf{X}\hat{\mathbf{X}}} + C_2}{\sigma_{\mathbf{X}}^2 + \sigma_{\hat{\mathbf{X}}}^2 + C_2}$, and $s(\mathbf{X}, \hat{\mathbf{X}}) = \frac{\sigma_{\mathbf{X}\hat{\mathbf{X}}} + C_3}{\sigma_{\mathbf{X}}\sigma_{\hat{\mathbf{X}}} + C_3}$. α , β , and γ are weighting parameters. $\mu_{\mathbf{X}}$ and $\sigma_{\mathbf{X}}$ denote the mean and standard deviation of \mathbf{X} , respectively. Similarly, $\mu_{\hat{\mathbf{X}}}$ and $\sigma_{\hat{\mathbf{X}}}$ denote the mean and standard deviation of $\hat{\mathbf{X}}$, respectively. $\sigma_{\mathbf{X}\hat{\mathbf{X}}}$ is the covariance between $\hat{\mathbf{X}}$ and \mathbf{X} . C_1 , C_2 , and C_3 are constants. Further, Eq. (5) can be simplified when $\alpha = \beta = \gamma = 1$ and $C_3 = \frac{C_2}{2}$ as

$$\text{SSIM} = \frac{(2\mu_{\mathbf{X}}\mu_{\hat{\mathbf{X}}} + C_1)(2\sigma_{\mathbf{X}\hat{\mathbf{X}}} + C_2)}{(\mu_{\mathbf{X}}^2 + \mu_{\hat{\mathbf{X}}}^2 + C_1)(\sigma_{\mathbf{X}}^2 + \sigma_{\hat{\mathbf{X}}}^2 + C_2)} \quad (6)$$

In comparison, SSIM [135] is reported to reflect visual quality better than PSNR. Generally, PSNR and SSIM [135] are combined to assess the quality of the restored image when the corresponding ground truth image is available.

3) *IFC* [136]: The information fidelity criterion (IFC) [136] is a full-reference metric that assesses the quality of images based on natural scene statistics.¹⁰ Research shows that the statistics of the space formed by natural images can be characterized using various models (*e.g.*, the Gaussian scale mixtures). Generally, distortions would disturb the statistics of natural scenes and make images unnatural. According to these observations, Sheikh *et al.* [136] propose to measure the visual quality of an image via jointly using the natural scene and distortion models to quantify the mutual information between the test image and reference. Overall, the IFC [136] performs well for the quality assessment of super-resolved images [140].

4) *LPIPS* [137]: The learned perceptual image patch similarity (LPIPS) [137] is a learned metric for reference-based image quality assessment.¹¹ More specifically, LPIPS [137] is obtained via computing the l_2 distance between the reference and the test image in a deep feature space, which shows a good agreement with human judgments.

5) *NIQE* [138]: The natural image quality evaluator (NIQE) is a completely blind metric without the knowledge of human judgments or distortions [138].¹² The multivariate Gaussian (MVG) model is used to fit the “quality-aware” features extracted from images. More specifically, the features include the parameters of the generalized Gaussian distribution (GGD) and the asymmetric generalized Gaussian distribution (AGGD) that characterize the behavior of image patches. Then, the quality of an image is measured using the distance between the two MVG models fitting natural images and the evaluated image.

6) *PIQE* [139]: The perception-based quality evaluator (PIQE) is a no-reference image quality assessment metric [139].¹³ Considering that the attention of human visual system

¹⁰The source code of IFC [136] is available at https://live.ece.utexas.edu/research/Quality/index_algorithms.htm

¹¹The source code of LPIPS [137] is available at <https://github.com/richzhang/PerceptualSimilarity>

¹²The source code of NIQE [138] is available at https://live.ece.utexas.edu/research/Quality/index_algorithms.htm

¹³The implementation of PIQE [139] is included in Matlab as <https://www.mathworks.com/help/images/ref/piqe.html>

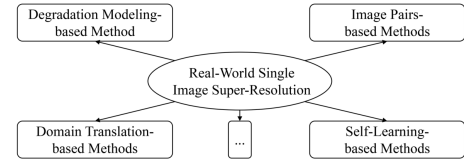


Fig. 2. The taxonomy of existing real-world single image super-resolution techniques.

(HVS) is highly directed towards spatially active regions, the test image is divided into non-overlapping blocks and block-level analysis is conducted to identify distortion and grade quality. Therefore, PIQE [139] can provide a spatial quality map. The overall quality of the evaluated image can be obtained by pooling the block level quality scores.

7) *NRQM* [116]: This is a learned no-reference quality metric (NRQM) for assessing super-resolved images [116].¹⁴ To predict the perceptual scores of super-resolved images, three groups of statistical features including local frequency features, global frequency features, and spatial features are extracted. The selected features cover the distribution of discrete cosine transform coefficients, the distribution of wavelet coefficients, the spatial discontinuity property of pixel intensity, *etc.* On this basis, three regression forests are used to model these features independently and their results are combined linearly to estimate the final perceptual score. These three forests and the linear regression model are trained on a large-scale dataset of super-resolved images with perceptual scores. Overall, the visual quality predicted by NRQM [116] matches subjective evaluation well on SR results.

IV. TECHNOLOGIES AND METHODS

Researchers have been studying the SISR methods for practical applications. Especially with the SR performance on synthetic data becoming better and better, more and more attention has been paid to RSISR. Fig. 2 presents the overall taxonomy of existing RSISR techniques. Note that we focus more on deep learning-based methods. According to the primary principles and characteristics of existing RSISR methods, we group them into four categories, *i.e.*, degradation modeling-based methods [88]–[98], image pairs-based methods [79]–[87], domain translation-based methods [99]–[110], and self-learning-based methods [94], [111]–[115]. Fig. 3 and Table III summarize existing RSISR methods. It is worth noting that one method may belong to different categories when it is viewed from different perspectives. The following sections introduce these methods in detail.

A. Degradation Modeling-based Methods

Compared with the SR of synthetic LR images, one of the main challenges for RSISR is that the degradation model (*i.e.*, the $D(\cdot)$ in Eq. (1)) is unknown. Generally, the degradation parameter set is necessary to design the objective function for reconstruction-based SISR methods derived from the

¹⁴The source code of NRQM [116] is available at <https://github.com/chaoma99/sr-metric>

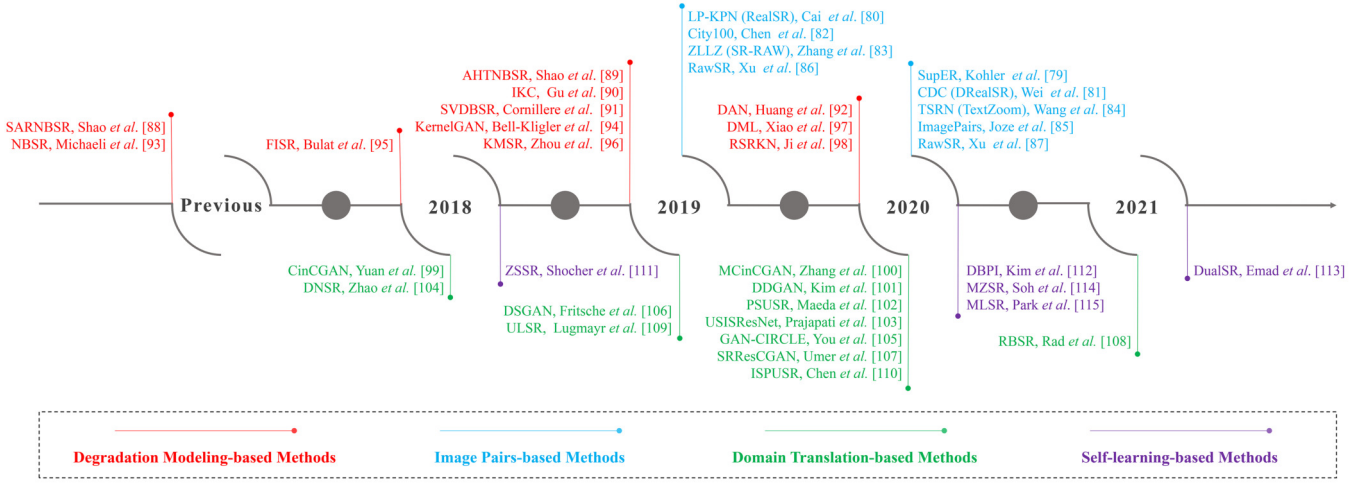


Fig. 3. Milestones of RSISR methods.

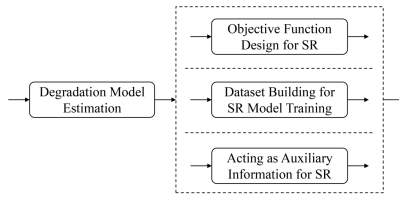


Fig. 4. The general idea of degradation modeling-based methods.

Maximum a Posteriori (MAP) estimation. For learning-based methods that aim to obtain the mapping from LR images to their HR counterparts, the degradation parameter set is crucial for building training datasets. Therefore, as presented in Fig. 4, an intuitive way is to estimate the degradation parameter of the LR input prior to super-resolving or to iteratively optimize the degradation parameter and the super-resolved image. Eq. (3)) shows the commonly used degradation model, in which the blur kernel \mathbf{B} and noise \mathbf{n} are unknowns. The exploration by Efrat et al. [141] shows that an accurate blur model is more important to the success of SR than a sophisticated image prior, in particular for real-world images. As highlighted in [141], most of the existing degradation modeling-based methods focus on the recovery of the blur kernel.¹⁵

RSISR is a severely ill-posed problem. Shao et al. [88] formulate this kind of task as an energy minimization problem and jointly optimize the nonparametric blur kernel and the intermediate super-resolved image. Mathematically, the objective function for blur kernel estimation is defined as

$$\min_{\mathbf{X}, \mathbf{b}} \lambda \|\mathbf{SBX} - \mathbf{Y}\|_2^2 + \mathfrak{R}(\mathbf{X}, \mathbf{b}) + \eta \|\mathbf{BX} - \tilde{\mathbf{X}}\|_2^2 \quad (7)$$

where λ and η are parameters for balancing different terms. $\tilde{\mathbf{X}}$ denotes the super-resolved image generated by a non-blind learning-based method, and \mathbf{b} denotes the blur kernel corresponding to the blur matrix \mathbf{B} . $\mathfrak{R}(\mathbf{X}, \mathbf{b})$ represents the

direct $bi\text{-}l_0\text{-}l_2$ -norm regularization term for the intermediate super-resolved image \mathbf{X} and the blur kernel \mathbf{b} , which is beneficial to the accurate estimation of \mathbf{b} . After iteratively optimizing the \mathbf{X} and \mathbf{b} in Eq. 7, the estimated blur kernel $\hat{\mathbf{b}}$ can be combined with non-blind SR methods to produce an HR estimate. In [89], Shao et al. introduce the l_α -norm-based adaptive heavy-tailed image prior to further improve the above approach. The studies in [88] and [89] demonstrate that, with the aid of effective constraints, the iterative optimization of the blur kernel and the super-resolved image is good for the accuracy of blur kernel estimation.

Different from the above numerical optimization-based approaches [88], [89], the blur kernel and the super-resolved image can also be jointly optimized using deep neural networks [90]–[92]. Generally, the mismatch of blur kernels would result in artifacts in the super-resolved image, e.g., over-smoothing or over-sharpening. Based on this observation, Gu et al. [90] and Cornillere et al. [91] propose to progressively correct the inaccurate kernel according to the quality of the super-resolved image.¹⁶ More specifically, they develop degradation-aware SR networks to produce HR images, in which the blur kernel is utilized as auxiliary information for SR. Meanwhile, corresponding deep neural networks are designed to correct the kernel with the guidance of the intermediate SR result. Unlike previous approaches [90], [91] that combine two or more networks, Huang et al. [92] develop a deep alternating network (DAN) for RSISR, in which the iterative optimization process between the super-resolved image and the blur kernel is unfolded to an end-to-end trainable network.¹⁷ DAN [92] consists of a chain of alternately stacked restorers and estimators, which are responsible for the restoration of the HR image and the estimation of the blur kernel, respectively. For the above methods, the super-resolved image and the blur kernel corresponding to the LR input are iteratively refined. After

¹⁶The source code of IKC [90] is available at <https://github.com/yuanjunchai/IKC>

¹⁷The source code of DAN [92] is available at <https://github.com/greatlog/DAN>

¹⁵In some cases, the noise is not explicitly characterized. Natural image priors are generally incorporated to suppress noise.

TABLE III
AN OVERVIEW OF EXISTING WORKS ON RSISR.

Methods	Published	Category	Keywords
SupER	TPAMI-2020 [79]	Image pairs-based	Benchmarking super-resolution on real data
LP-KPN (RealSR)	ICCV-2019 [80]	Image pairs-based	Laplacian pyramid-based kernel prediction network
CDC (DRealSR)	ECCV-2020 [81]	Image pairs-based	Component divide-and-conquer model, Gradient weighted loss
CameraSR (City100)	CVPR-2019 [82]	Image pairs-based	SR from the perspective of camera lenses
ZLLZ (SR-RAW)	CVPR-2019 [83]	Image pairs-based	RAW sensor data, Contextual bilateral loss
TSRN (TextZoom)	ECCV-2020 [84]	Image pairs-based	Sequential residual block, Central alignment module, Gradient profile loss
ImagePairs	CVPRW-2020 [85]	Image pairs-based	A new data acquisition technique for gathering real image data
RawSR	CVPR-2019 [86], TPAMI-2020 [87]	Image pairs-based	Two-branch structure, Raw image, Color correction
SARNBSR	ICIG-2015 [88]	Degradation modeling-based	Blur kernel estimation, Bi- l_0 - l_2 -norm regularization
AHTNBSR	JMIV-2019 [89]	Degradation modeling-based	Adaptive heavy-tailed image priors, Nonparametric blur kernel estimation
IKC	CVPR-2019 [90]	Degradation modeling-based	Iterative kernel correction, Spatial feature transform
SVDBSR	TOG-2019 [91]	Degradation modeling-based	Degradation-aware SR network, Kernel discriminator network
DAN	NeurIPS-2020 [92]	Degradation modeling-based	SR image restorer, Blur kernel estimator, End-to-end trainable
NBSR	ICCV-2013 [93]	Degradation modeling-based	Kernel estimation, Recurrence of small image patches
KernelGAN	NeurIPS-2019 [94]	Degradation modeling-based	Deep internal learning, Cross-scale recurrence property, GAN, Image-specific SR-kernel
FISR	ECCV-2018 [95]	Degradation modeling-based	High-to-low GAN, Low-to-high GAN, Unpaired LR and HR images
KMSR	ICCV-2019 [96]	Degradation modeling-based	Realistic blur kernels, Blur kernel pool augment, GAN
DML	ACCV-2020 [97]	Degradation modeling-based	Realistic HR-LR image pair synthesis, Pixel-wise spatially variant degradation kernel
RSRKN	CVPRW-2020 [98]	Degradation modeling-based	Degradation framework, Kernel estimation, Noise injection, GAN
CinCGAN	CVPRW-2018 [99]	Domain translation-based	Unsupervised learning, Cycle-in-cycle network structure, GAN
MCinCGAN	TIP-2020 [100]	Domain translation-based	Unsupervised learning, Multiple cycle-in-cycle network structure, GAN
DDGAN	CVPRW-2020 [101]	Domain translation-based	Unsupervised learning, Unknown degradation, Cycle-in-cycle GAN, Domain discriminator
PSUSR	CVPR-2020 [102]	Domain translation-based	Unpaired kernel/noise correction network, Pseudo-paired SR network, GAN
USISResNet	CVPRW-2020 [103]	Domain translation-based	Unsupervised learning, GAN, Mean Opinion Score-based loss function
DNSR	arXiv-2018 [104]	Domain translation-based	Unsupervised degradation learning, Bidirectional structural consistency, Bi-cycle network
GAN-CIRCLE	TMI-2020 [105]	Domain translation-based	Computed tomography, CycleGAN
DSGAN	ICCVW-2019 [106]	Domain translation-based	Frequency separation, Unsupervised learning, GAN
SRResCGAN	CVPRW-2020 [107]	Domain translation-based	Image observation model, Domain learning, GAN
RBSR	WACV-2021 [108]	Domain translation-based	Bicubically down-sampled images, GAN
ULSR	ICCVW-2019 [109]	Domain translation-based	Unsupervised learning, Unpaired data, GAN
ISPUSR	CVPRW-2020 [110]	Domain translation-based	Unsupervised image translation, Supervised SR, Collaborative training
ZSSR	CVPR-2018 [111]	Self-learning-based	Zero-shot, Internal recurrence, Deep internal learning, Image-specific CNN
DBPI	SPL-2020 [112]	Self-learning-based	Unified internal learning, Downscaling/SR network, Dual back-projection loss
DualSR	WACV-2021 [113]	Self-learning-based	Zero-shot, Dual-path architecture, GAN, Masked interpolation loss
MZSR	CVPR-2020 [114]	Self-learning-based	Meta-transfer learning, Large-scale training, External and internal information
MLSR	ECCV-2020 [115]	Self-learning-based	Meta-learning, Patch-recurrence property

joint optimization, the refined blur kernel and the super-resolved image are supposed to be more accurate.

Previous studies have shown that natural image priors such as patch recurrence property are useful for degradation modeling. In [93], Michaeli *et al.* point out that the Point Spread Function (PSF) is not the optimal blur kernel, and they further propose to obtain the principled MAP estimate of the blur kernel via maximizing the similarity of recurring image patches across scales of the LR input.¹⁸ The estimated blur kernel can be used to degrade the LR input or natural HR images artificially. In this way, the blur kernel estimation approach is smoothly plugged into both self-example-based and external-example-based SR approaches [47], [54]. The results in [93] show that the accuracy enhancement of blur kernel estimation leads to an obvious improvement of SR performance on synthetic as well as real-world images.

Degradation modeling is also vitally important for deep learning-based SR approaches. Deep convolutional neural networks (CNN)-based SISR approaches usually achieve state-of-the-art (SOTA) results on standard benchmarks. Nevertheless, their performance is limited when applied to real-world images. The main reason is that the kernel (e.g., “bicubic” kernel) used to generate training data is significantly different from the blur in a real scenario. To address this problem, some recently presented deep learning-based RSISR methods [94]–[98] adopt the pre-estimated degradation parameters to generate samples for model training. For example, inspired by [93], Bell-Kligler *et al.* [94] develop an image-specific internal-GAN (*i.e.*, KernelGAN) to learn the internal distribution of patches.¹⁹ The KernelGAN [94] is trained solely using the LR test image, making its discriminator unable to differentiate the patch distribution of the original LR input from that of the degraded version of the LR image produced by the generator. After the joint training with the discriminator, the generator can well characterize the degradation process with an image-specific kernel. Then, the LR test image and its degraded version generated by the generator form paired data for SR model training. Bulat *et al.* [95] train a generative adversarial network (GAN)-based degradation model from unpaired HR and LR face images, and then use the learned network to generate image pairs for SR network training.²⁰ Zhou *et al.* [96] propose to obtain a group of realistic blur kernels from real-world photographs and a GAN is trained on them to augment the pool of realistic blur kernels.²¹ With the augmented kernel pool, more realistic and diverse LR-HR image pairs can be constructed to train the SR model. Analogously, Xiao *et al.* [97] model spatially variant degradation via learning a set of basis blur kernels and corresponding pixel-wise weights from real-world image pairs. The learned realistic degradation model is then used to generate pseudo-realistic LR-HR image pairs. More recently,

¹⁸The project homepage of NBSR [93] is at <http://www.wisdom.weizmann.ac.il/~vision/BlindSR.html>

¹⁹The source code of KernelGAN [94] is available at <https://github.com/sefibk/KernelGAN>

²⁰The source code of FISR [95] is available at <https://github.com/jingyang2017/Face-and-Image-super-resolution>

²¹The source code of KMSR [96] is available at <https://github.com/IVRL/Kernel-Modeling-Super-Resolution>

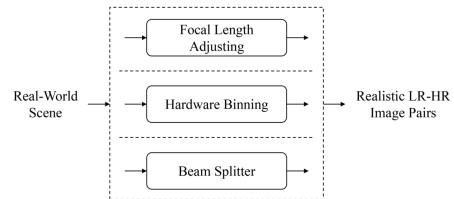


Fig. 5. Existing solutions to construct realistic LR-HR image pairs.

Ji *et al.* [98] take this idea one step further and develop an effective degradation framework using various realistic blur kernels and noise distributions, winning the *NTIRE 2020 Challenge on Real-World Image Super-Resolution* [122].²² The outstanding performance of degradation modeling-based RSISR methods demonstrates that degradation modeling is meaningful and this kind of approach is a feasible solution to the SR of real-world images.

B. Image Pairs-based Methods

Although paired LR-HR training data can be synthesized from high-quality images according to pre-defined degradation models [96], [98], deriving explicit realistic degradation models from real-world images is challenging. To deal with this problem, researchers [79]–[85] propose to directly collect the images of the same scene with different resolutions, which are used to construct realistic LR-HR image pairs for RSISR model training. Overall, as illustrated in Fig. 5, currently there are three main ways to collect real-world images for dataset building, including the focal length adjusting-based approach [80]–[84], the hardware binning-based approach [79], and the beam splitter-based approach [85]. The representative realistic datasets built with the above image collection approaches are described in Section III-A. Therefore, this section focuses on the RSISR models developed on these real-world datasets. Intuitively, given LR-HR image pairs, nearly all existing supervised SR methods (e.g., SRCNN [67], VDSR [68], EDSR [70], RDN [74], SRGAN [69], *etc.*) can be adopted to learn the mapping from LR images to their HR counterparts. The mapping learned from realistic datasets is supposed to apply to the SR of real-world images. However, in fact challenges remain.

For instance, the degradation kernels of real-world images are generally non-uniform, varying with the depth in a real scene. Thus, training an SR model that treats all pixels the same way as most previous deep CNN-based SR approaches may not be the optimal solution. For this problem, Cai *et al.* [80] propose the LP-KPN, which combines the Laplacian pyramid with the pixel-wise kernel prediction network (KPN), achieving good SR performance and high efficiency.²³ Another challenge that cannot be ignored is the misalignment between LR and HR image pairs in the collected realistic datasets. Although image registration is performed

²²The source code of RSRKN [98] is available at <https://github.com/jixiaozhong/RealSR>

²³The source code of LP-KPN [80] is available at <https://github.com/csjaic/RealSR>

to align realistic image pairs, misalignment is unavoidable. As a consequence of misalignment, blurring artifacts may be introduced in the reconstructed HR images when using these datasets to train the SR model with pixel-to-pixel losses (*e.g.*, l_1 and l_2). Inspired by the Contextual Loss [142] and the edge-preserving bilateral filter [143], Zhang *et al.* [83] propose the Contextual Bilateral loss (CoBi) to resolve this issue.²⁴ CoBi integrates the pixel-level information and spatial pixel coordinates to measure image similarity. Moreover, two spaces including RGB image patches and pre-trained perceptual-features (*e.g.*, VGG-19 [144]) are jointly considered in CoBi to improve performance further. It is demonstrated that CoBi is robust to the mild misalignment in the realistic image pairs for supervised SR model training. Considering that pixel-wise losses are generally more focused on smoothing flat regions and sharpening edges while neglecting the recovery of realistic details of textures to some extent, Wei *et al.* [81] develop a Component Divide-and-Conquer (CDC) SR model for real-world images.²⁵ More specifically, the flat, edge, and corner components are first predicted by three component-attentive blocks respectively in CDC and then they are aggregated to produce the final SR image based on the learned component-attentive maps. To achieve this goal, a gradient-weighted loss that can adapt the model training to the reconstruction difficulties of different image components is applied. The results on RealSR [80] and DRealSR [81] prove the superiority and generalization capability of CDC [81]. Given a dataset containing raw and color images, learning a mapping from LR raw images to HR color images using deep neural networks is an intuitive approach to exploit raw images for SR. However, one raw image could correspond to a set of color images because it does not have the information for the processes (*e.g.*, color correction) within the image signal processing system, making the above naive way do not work well. To address this problem, Xu *et al.* [86], [87] design a two-branch CNN which jointly exploits the LR raw data and corresponding LR color image to recover fine structures and high-fidelity color appearances.

In addition to the above challenges shared by almost all real-world images, the SR of certain kinds of images (*e.g.*, text images, remote sensing images, and medical images) usually has a particularity. Therefore, specific SR models should be designed for these scenarios. For example, the TSRN developed by Wang *et al.* [84] is an SR network for real scene text images.²⁶ To leverage the strong sequential characteristics of text images, the Bi-directional LSTM (BLSTM) mechanism is added to basic residual blocks. In order to address the misalignment problem in the realistic text image dataset TextZoom, TSRN [84] introduces a spatial transform network-based central alignment module in the front of the network. Furthermore, aiming at enhancing the shape boundary of characters, a gradient prior loss is combined with the l_2

²⁴The source code of ZLLZ [83] is available at <https://github.com/ceciliavision/zoom-learn-zoom>

²⁵The source code of CDC [81] is available at <https://github.com/xiezw5/Component-Divide-and-Conquer-for-Real-World-Image-Super-Resolution>

²⁶The source code of TSRN [84] is available at <https://github.com/JasonBoy1/TextZoom>

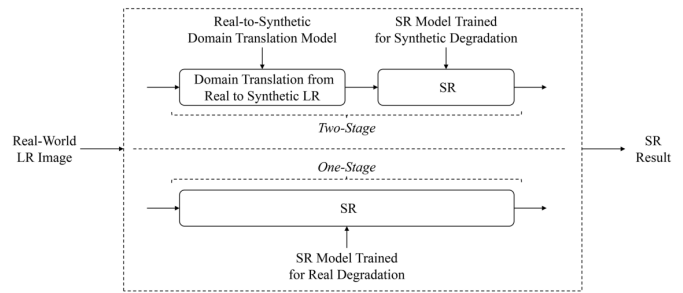


Fig. 6. The general idea of domain translation-based methods.

loss to train TSRN. It is demonstrated that the SR of real-world text images using TSRN does increase the recognition accuracy. Predictably, in some cases, SR can also benefit other computer vision tasks, *e.g.*, objection detection [5] and semantic segmentation [4].

C. Domain Translation-based Methods

As introduced in Sections III-A and IV-B, it is hard to obtain real-world datasets with well-aligned LR-HR image pairs. More often than not, what we have are only LR images for model training in practical applications. Or better yet, a set of HR images are available for reference besides LR training images, but there is no one-to-one correspondence between LR and HR images. The supervised approaches no longer apply in these cases due to the lack of paired samples. Previous studies [99]–[107], [107]–[110] demonstrate that domain translation is a feasible solution to deal with this problem. For this kind of RSISR approach, real-world LR images, synthetic LR images (also known as clean LR images or ideal LR images), and HR images are thought to be in different domains. Consequently, the SR of real-world images converts to the translation from the real-world LR image domain (RLRD) to the HR image domain (HRD). Overall, as presented in Fig. 6, there are two main ways to cross RLRD to HRD, *i.e.*, the two-stage and the one-stage approaches, and the most notable difference lies in whether the synthetic LR image domain (SLRD) is used as a relay station.

Most existing SISR approaches are trained using synthetic data, thereby achieving excellent performance on clean LR images. As is known to all, there is a noticeable domain gap between SLRD and RLRD, causing the degradation of SR accuracy on real-world images. Intuitively, one can mitigate this performance degradation via reducing the domain gap, which is how the two-stage domain translation-based RSISR approaches work. As shown in Fig. 6, the two-stage approaches generally include two main steps, *i.e.*, domain translation and SR. Usually, generic SR methods are adopted in the SR reconstruction phase, so as to benefit from pre-trained SR models learned from large-scale datasets. The Cycle-in-Cycle GAN (CinCGAN) developed by Yuan *et al.* [99] is a representative of this kind of RSISR method. More specifically, CinCGAN [99] first uses a domain translation network to map realistic LR images in RLRD into the SLRD, and then a pre-trained deep SR network with the ideal

degradation assumption is stacked to upscale the translation result to the desired size. Finally, the domain translation and SR networks are end-to-end fine-tuned. Inspired by CycleGAN [145], the domain translation network in CinCGAN [99] is trained to map realistic LR inputs to synthetic LR images (*i.e.*, “bicubic”-downsampled images) using unpaired training data, which usually can suppress the artifacts such as noise in real-world LR images to make them more suitable for the following SR network. Results show that the CinCGAN [99] trained with unpaired data achieves comparable SR performance as supervised methods. In MCinCGAN [100], the CinCGAN [99] is improved via introducing a progressive multi-cycle framework for large-scale upsampling and a new constraint to suppress the color fluctuation in training. For more stable model training and better SR performance, the DDGAN developed by Kim *et al.* [101] further combines the pixel-wise loss, the VGG feature loss, and the SSIM loss to measure similarity.²⁷ Meanwhile, a domain discriminator that takes the noise, texture, and color into consideration simultaneously is proposed to make the generated image more consistent with the target domain distribution. More recently, Maeda *et al.* [102] propose an end-to-end trainable framework UISRPS to jointly optimize the domain translation network and the SR network, achieving excellent SR results on real-world face images and aerial images. Benefiting the architecture, it is convenient to integrate existing SR networks and pixel-wise loss functions into UISRPS [102].

Different from the two-stage methods mentioned above, the one-stage domain translation-based RSISR frameworks aim to produce a super-resolved image directly from the real-world LR input, as presented in Fig. 6. How to learn the translation mapping from RLRD to HRD without real LR-HR image pairs is the crucial issue. Prajapati *et al.* [103] propose to train a GAN-based network USISRNet to upsample real-world images.²⁸ Since only unpaired LR and HR training images are available, USISRNet is optimized through unsupervised learning. Beyond the standard GAN losses, a pixel-wise content loss, a Total-Variation loss, and a quality assessment loss are combined to optimize USISRNet. The content loss makes the SR result be not far from the bicubically upsampled version, thus preserving the primary content of the LR image. The Total-Variation loss is integrated to suppress the noise and artifacts. For better perceptual quality of the super-resolved image, the learned Mean Opinion Score is used to construct the quality assessment loss. Thanks to the combination of multiple losses, USISRNet [103] achieves good generalization capacity. Inspired by CycleGAN [145], some researchers propose to learn the direct relationship between RLRD to HRD using cycle consistency-constrained GANs [104], [105].²⁹ Given an LR image, the LR-to-HR generator (*i.e.*, RLRD to HRD) is trained to reconstruct a vivid HR image that can be returned to the LR input by

the corresponding HR-to-LR generator (*i.e.*, HRD to RLRD). Conversely, an HR image should be well recovered by the LR-to-HR generator from its downsampled version produced by the HR-to-LR generator. After the joint training of the two generators and corresponding discriminators, the LR-to-HR generator models the direct mapping from RLRD to HRD and it is used to reconstruct HR images from realistic LR images.

Considering that learning the end-to-end translation between RLRD to HRD from unpaired LR-HR data is challenging, part of the one-stage domain translation-based RSISR methods [106]–[110] also use the synthetic LR image as a bridge in the training phase. Given unpaired realistic LR and HR images, Fritsche *et al.* [106] first bicubically downsample HR images. Bicubically downsampled results are then translated into the realistic domain to make them follow real scene characteristics, using a standard GAN-based domain translation network trained on the bicubically downsampled images and realistic LR images in an unsupervised fashion. Taking the pseudo-realistic LR images and corresponding HR images as training sample pairs, the ESRGAN [146] is trained for upsampling in a supervised manner. In order to generate images well matching the target distribution, both domain translation and SR networks are optimized with frequency separation-based loss functions.³⁰ More specifically, the color loss, the texture loss, and the perceptual loss are employed to the low-frequency component, the high-frequency component, and the whole image, respectively. Note that only the SR model is needed to upscale real-world images in the testing phase because it is trained on the image pairs that follow real-world image distribution. On this basis, recently Umer *et al.* [107] improve the GAN-based SR model following the real-world image observation model, thus exploiting the powerful regularization and optimization techniques simultaneously.³¹ Rad *et al.* [108] convert realistic LR images to bicubic look-alike images based on their copying mechanism and bicubic perceptual loss. Different from the above works [106]–[108] which use a single direction domain translation model, Lugmayr *et al.* [109] and Chen *et al.* [110] propose to train a bi-directional domain translation model with the cycle consistency constraints for better robustness.

Overall, domain translation is an effective way to reduce the domain gap between synthetic and realistic data, thus improving the generalization capability of SR models on ever-changing real-world images. In contrast, the two-stage domain translation-based RSISR approaches can integrate synthetic data-trained SR models more elegantly, while the one-stage methods generally have lower complexity in the testing phase.

D. Self-Learning-based Methods

Most existing RSISR methods use external dataset (*i.e.*, paired or unpaired training data) to train SR models. Therefore, the SR performance is tightly bound to the consistency between testing data and training data. However, real-world

²⁷The source code of DDGAN [101] is available at <https://github.com/GT-KIM/unsupervised-super-resolution-domain-discriminator>

²⁸The source code of USISRResNet [103] is available at <https://github.com/kalpeshjp89/USISRResNet>

²⁹The source code of GAN-CIRCLE [105] is available at <https://github.com/charlesyou999648/GAN-CIRCLE>

³⁰The source code of DSGAN [106] is available at <https://github.com/ManuelFritsche/real-world-sr>

³¹The source code of SRResCGAN [107] is available at <https://github.com/RaoUmer/SRResCGAN>

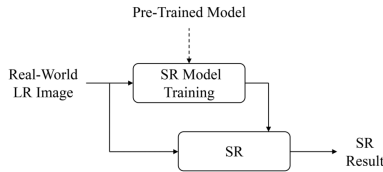


Fig. 7. The general idea of self-learning-based SR methods. Note that the pre-trained model is optional.

images do not always obey the characteristics of training data. In order to reduce the impact of the training–testing discrepancy on SR performance, researchers propose to exploit the internal information of the LR input to learn image-specific SR model as shown in Fig. 7.

The “Zero-Shot” SR (ZSSR) developed by Shocher *et al.* [111] is one of the representatives.³² The self-supervised approach ZSSR [111] is based on the cross-scale internal recurrence of information, which is a common property of natural images. More specifically, an eight-layer CNN is trained to model image-specific LR–HR relations in the testing phase, using the example pairs extracted from the LR test image and its degraded version. In consideration of the insufficiency of training data (the test image only), data augmentation is adopted when extracting image-specific LR–HR pairs. Since ZSSR [111] can adapt itself to different testing images, it achieves excellent SR performance on real-world images, whose degradation process is non-ideal and unknown. Again based on the cross-scale recurrence property, Bell-Kligler *et al.* [94] propose to train an image-specific GAN (KernelGAN) to model the degradation process (*i.e.*, the blur kernel) of the input.¹⁹ Therefore, a fully self-supervised image-specific RSISR framework can be achieved when the blur kernel estimation module KernelGAN [94] is plugged into the reconstruction module ZSSR [111]. To jointly train the image-specific degradation and SR networks, Kim *et al.* [112] design a unified internal learning-based SR framework DBPI, consisting of an SR network and a downscaling network.³³ In the self-supervised training phase of DBPI, the SR network is optimized to reconstruct the LR input image from its downsampled version produced by the downscaling network. Meanwhile, the downscaling network is trained to recover the LR input image from its super-resolved version generated by the SR network. Similarly, Emad *et al.* [113] propose the DualSR that jointly optimizes an image-specific downsampler and corresponding upsampler. More specifically, DualSR [113] is trained with the cycle-consistency loss, the masked interpolation loss, and the adversarial loss using the patches from the test image. Results in [112], [113] show that the complementary training of the image-specific degradation and SR networks is beneficial to the reconstruction performance.

Although self-learning-based RSISR approaches such as ZSSR [111], KernelGAN [94], and DBPI [112] can be easily

³²The source code of ZSSR [111] is available at <https://github.com/assafshocher/ZSSR>

³³The source code of DBPI [112] is available at <https://github.com/prote376/DBPI-BlindSR>

adapted to LR input images, they generally have two main shortcomings due to the self-supervised training strategy. First, the optimization of SR models only utilizes the internal information of the LR input, while a great deal of external information is neglected. Second, these methods are usually time-consuming in the testing phase because of online training. To overcome these disadvantages, meta-learning is introduced into recent self-learning-based SR methods [114], [115]. Based on ZSSR [111], Soh *et al.* [114] present the meta-transfer learning for zero-shot SR (MZSR), which consists of three steps, *i.e.*, large-scale training, meta-transfer learning, and meta-test.³⁴ In order to ease the training of the SR network and the meta-learning, the large-scale training step first trains an eight-layer SR network with the pixel-wise l_1 loss on the large-scale dataset DIV2K [128]. The meta-transfer learning process aims to find a generic initial point for internal learning following the Model-Agnostic Meta-Learning [147], making the model can be quickly adapted to new image conditions within a few gradient updates. In the meta-test phase, the input test image is first degraded to produce example pairs for model parameter update, and then it is fed into the updated model to generate an SR result. Thanks to the meta-transfer learning strategy, MZSR [114] achieves competitive performance in terms of both the quality of the super-resolved image and the running time. In [115], Park *et al.* also propose to improve the performance of SOTA SR networks such as RCAN [73] using the meta-learning strategy, without changing the original architectures.³⁵ On the whole, meta-learning-based SR approaches have strengths in reconstruction quality, generalization capability, and processing efficiency.

V. COMPARISONS AMONG STATE-OF-THE-ARTS

In this section, we compare representative RSISR methods on benchmark datasets. More specifically, the selected competitors are ZSSR [111], KernelGAN [94], MZSR [114], DBPI [112], DAN [92], IKC [90], and SRResCGAN [107], covering multiple kinds of approaches mentioned in Section IV. For these SR approaches, we use the official models provided by authors in the comparison, and the upsampling factor is set to 2 or 4. Two benchmark datasets are tested, including the DIV2K [94] and RealSR [80]. As introduced in Section III-A, DIV2K [94] is a synthetic dataset with random kernels and RealSR [80] is a realistic dataset collected by adjusting the focal length.³⁶ In addition to the subjective quality comparison presented in Figs. 8–11, the SR results by different methods are objectively evaluated in Table IV on full-reference and no-reference image quality assessment metrics, including PSNR, SSIM [135], IFC [136], LPIPS [137], NIQE [138], PIQE [139], and NRQM [116]. Beyond reconstruction accuracy, the model size and execution speed are also significant for SR algorithms. Therefore, the number of parameters and running time are also presented in Fig. 12.

³⁴The source code of MZSR [114] is available at <https://www.github.com/JWSoh/MZSR>

³⁵The source code of MLSR [115] is available at <https://github.com/parkseobin/MLSR>

³⁶There are two subsets for testing in RealSR [80], *i.e.*, Canon and Nikon. We only use the 50 testing images in Canon in this comparison.

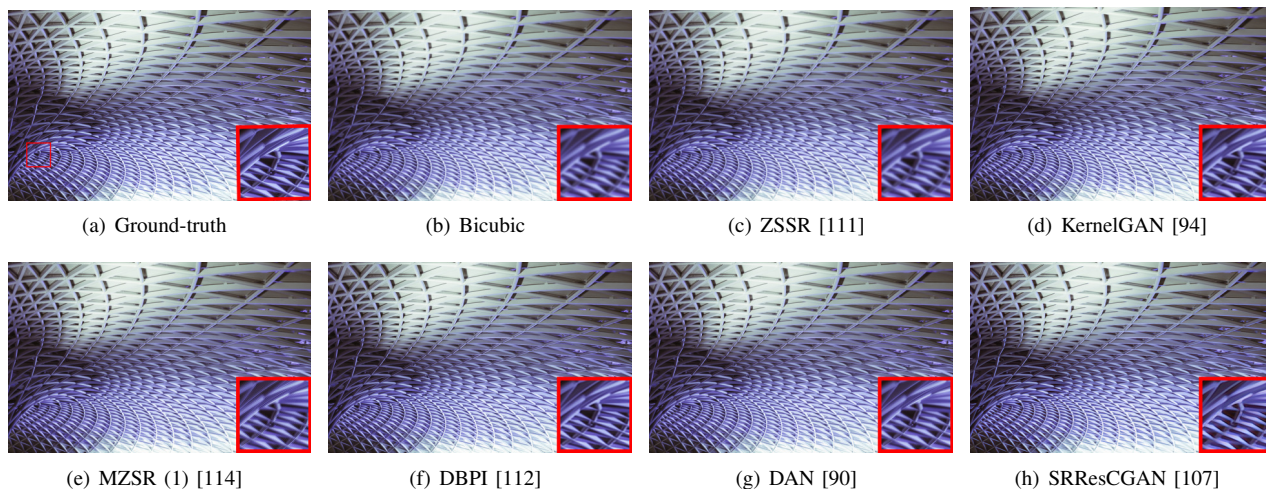


Fig. 8. Super-resolution results comparison ($\times 2$) on the image taken from DIV2K [94].

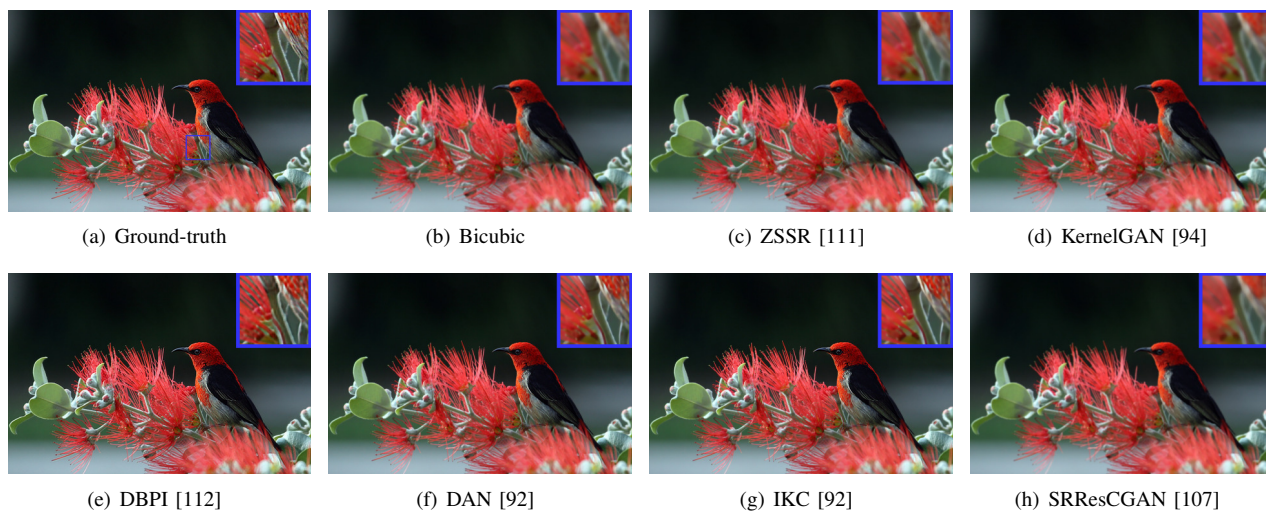


Fig. 9. Super-resolution results comparison ($\times 4$) on the image taken from DIV2K [94].

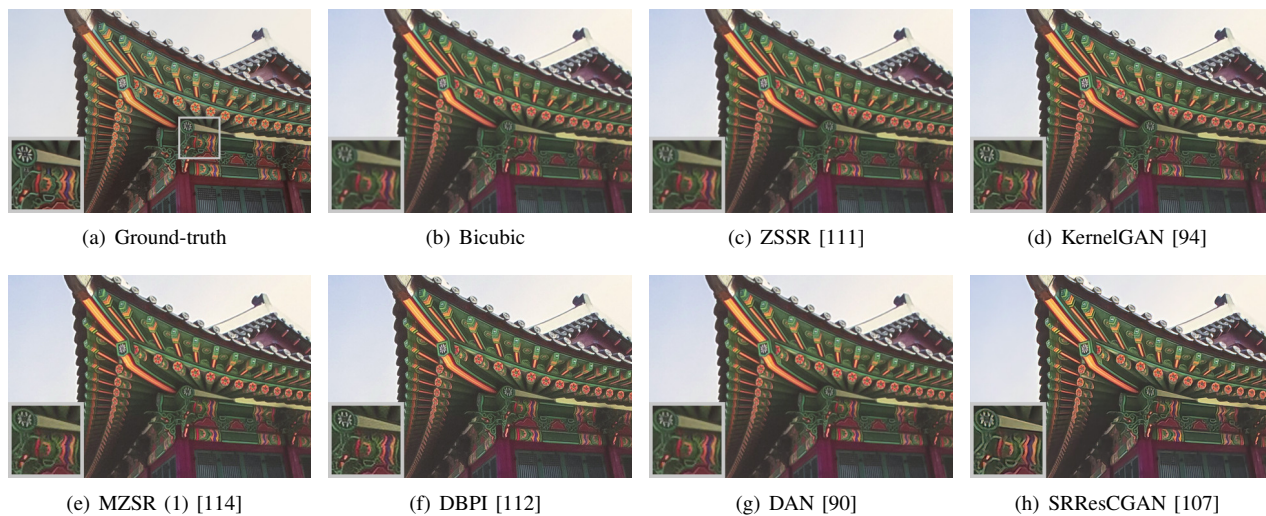


Fig. 10. Super-resolution results comparison ($\times 2$) on the image taken from RealSR [80].

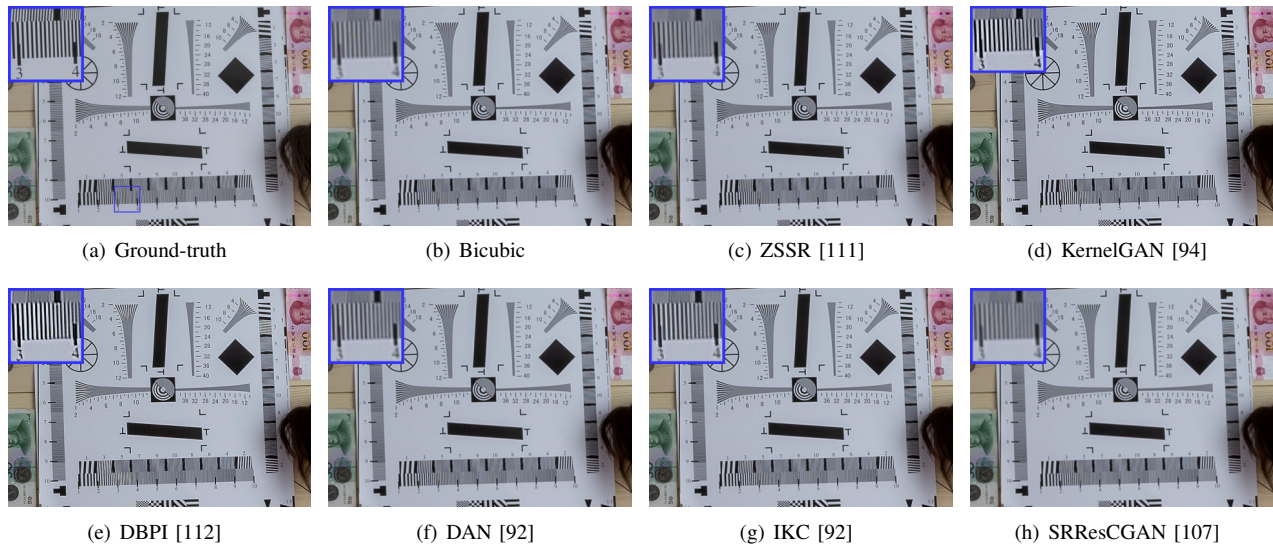


Fig. 11. Super-resolution results comparison ($\times 4$) on the image taken from RealSR [80].

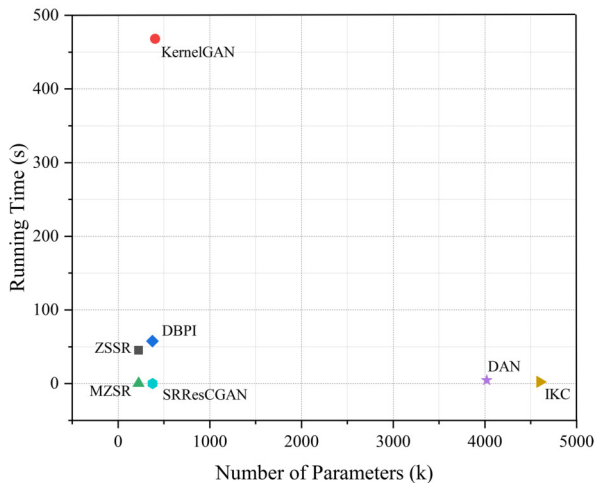


Fig. 12. The number of parameters and the average running time on the images taken from RealSR [80].

It is worth noting that the results shown in this section may be different from those in the original paper due to different settings of test environments, hyper-parameters, *etc.* The aim of these comparisons is not to find a winner in terms of accuracy or efficiency, but to indicate the current state of the research on RSISR. In fact, as is known to all, it is not easy to make a completely fair comparison among these competitors due to the complexity of settings. As far as we know, in particular, there is no uniform or universally accepted settings yet for the comparison of RSISR models.

We can make the following observations from the comparison results on visual quality, objective quality, and complexity. (i) Compared with conventional interpolation (*e.g.*, “Bicubic”), SR is undoubtedly a more effective way to obtain HR images. (ii) Overall, there is an obvious gap between the super-resolved image and the corresponding ground-truth in terms of visual effects, especially for texture and

edge regions. For example, some SR results suffer from over-smoothing or over-sharpening artifacts. (iii) There are some differences between subjective and objective assessment results. Moreover, the scores by different objective assessment metrics may not be necessarily consistent with each other. (iv) In general, self-supervised learning-based SR approaches have fewer parameters than the SR models trained on large-scale datasets, but take longer to produce upsampled images.

VI. CURRENT CHALLENGES AND FUTURE DIRECTIONS

The numerous studies reviewed in Sections III and IV demonstrate the great progress of the research on RSISR. In fact, however, there are still problems requiring further exploration. We discuss some of the challenges and promising directions for RSISR in this section.

A. Image Datasets

Overall, the data for SR model training may be equally as crucial as the SR techniques for the study on RSISR, especially for deep learning-based solutions. Several realistic datasets have been constructed in the past few years, significantly boosting the reconstruction performance. However, compared with the datasets for popular computer vision tasks such as classification and detection, the lack of realistic datasets for RSISR is still striking. Therefore, it is desired to build larger and more representative/targeted realistic datasets for RSISR with considering the limiting factors of imaging resolution in the future. Meanwhile, more accurate alignment of the images captured from the same scene with different resolutions is also needed.

B. SR Algorithms

Although the SR performance on real-world images is getting better and better, there is still a long way to go before applying RSISR algorithms to practical applications. First, the LR images captured in real scenarios are likely to suffer from

TABLE IV
THE PERFORMANCE OF REPRESENTATIVE RSISR ALGORITHMS ON DIV2K [94] AND REALSR [80] DATASETS.

<i>Method</i>	<i>Scale</i>	PSNR \uparrow (dB)	SSIM \uparrow [135]	IFC \uparrow [136]	NIQE \downarrow [138]	PIQE \downarrow [139]	NRQM \uparrow [116]	LPIPS \downarrow [137]
<i>Performance on the synthetic dataset DIV2K [94]</i>								
Bicubic	$\times 2$	27.24	0.7846	3.022	5.196	79.90	3.273	0.3631
	$\times 4$	23.89	0.6478	1.092	6.310	95.26	3.043	0.5645
ZSSR [111]	$\times 2$	27.51	0.7925	3.000	5.068	80.06	3.435	0.3477
	$\times 4$	24.05	0.6550	1.132	5.824	90.29	3.109	0.5257
KernelGAN [94]	$\times 2$	28.84	0.8379	3.720	5.099	72.17	3.920	0.2929
	$\times 4$	24.76	0.6799	1.245	5.886	88.72	3.610	0.4980
MZSR (1) [114]	$\times 2$	26.69	0.7889	2.515	5.627	35.97	4.112	0.2630
DBPI [112]	$\times 2$	29.55	0.8657	4.084	5.239	50.61	4.844	0.2641
	$\times 4$	24.92	0.7035	1.385	5.163	70.74	4.980	0.4039
DAN [92]	$\times 2$	31.06	0.8848	5.076	4.041	56.14	3.519	0.1667
	$\times 4$	26.07	0.7305	1.758	5.570	82.28	3.157	0.4045
IKC [90]	$\times 4$	25.41	0.7255	1.691	5.140	79.72	3.869	0.3977
SRResCGAN [107]	$\times 2$	26.15	0.7486	1.808	3.717	35.88	4.976	0.2463
	$\times 4$	24.00	0.6497	1.024	5.038	74.27	3.054	0.5054
<i>Performance on the real-world dataset RealSR [80]</i>								
Bicubic	$\times 2$	30.27	0.8736	1.921	5.569	83.90	2.731	0.2095
	$\times 4$	25.74	0.7413	0.890	6.228	92.53	2.802	0.4666
ZSSR [111]	$\times 2$	30.56	0.8786	1.949	5.376	81.09	2.749	0.1756
	$\times 4$	25.83	0.7434	0.897	4.971	83.01	2.797	0.3503
KernelGAN [94]	$\times 2$	30.24	0.8907	2.106	5.384	77.10	2.769	0.1338
	$\times 4$	24.09	0.7243	0.897	4.918	78.96	3.559	0.2981
MZSR (1) [114]	$\times 2$	27.96	0.8160	1.520	5.887	38.83	2.868	0.2105
DBPI [112]	$\times 2$	27.86	0.8285	1.876	5.698	54.87	2.995	0.1777
	$\times 4$	22.36	0.6562	0.851	5.640	70.58	5.056	0.3106
DAN [92]	$\times 2$	30.63	0.8815	1.959	4.387	68.68	2.745	0.1314
	$\times 4$	26.20	0.7598	0.966	6.096	90.57	2.834	0.4095
IKC [90]	$\times 4$	25.60	0.7488	0.944	4.845	82.75	2.927	0.3188
SRResCGAN [107]	$\times 2$	26.26	0.7983	1.573	3.786	39.40	4.129	0.2090
	$\times 4$	25.84	0.7459	0.900	5.009	74.45	2.795	0.3746

distinctly different degradations, challenging existing RSISR algorithms. Therefore, it is necessary to make RSISR models can adapt themselves to ever-changing real-world images. Second, most existing RSISR approaches are with a large model (*e.g.*, a deep network), thereby requiring vast computing resources/time for forward inference and plenty of space for parameters storage. However, these resources are generally limited in real-world applications. Hence, how to achieve lightweight design and implementation of SR models without significant performance degradation is a primary challenge. Third, it is hard to obtain paired training data, even unpaired data or relevant HR references in some cases. Thus it is promising to develop RSISR models that can be run with unpaired training data or even the LR input only. Moreover, how to leverage fewer models to meet personalized and multifunctional demands (*e.g.*, the need for arbitrary upscaling factors and the preference to perceptual quality) of users

deserves further investigation.

C. Evaluation Criteria

The evaluation criteria are vitally crucial for the research on computer vision tasks. On the one hand, the design of objective functions is generally guided by the evaluation criteria. For example, the l_2 loss is prevalent for image/video restoration tasks because it is highly correlated to the commonly used quality assessment metric PSNR. On the other hand, evaluation criteria are needed to make comparisons among different approaches, thus continuously advancing techniques. As previously mentioned, currently the PSNR and SSIM are the two of the most popular evaluation metrics for SR. However, previous studies show that they are unable to measure the visual quality of super-resolved images accurately. In addition, PSNR and SSIM are full-reference evaluation metrics that cannot be adopted in practical applications.

Therefore, developing more suitable evaluation criteria for RSISR is a crucial and urgent research problem. On the whole, task-specific evaluation metrics are needed. That is, we have to take the goals and characteristics of RSISR into consideration while developing evaluation criteria. For example, the common targets include smoothness preserving for flat areas, detail enhancing for textures, sharpening for edges, *etc.* Correspondingly, an evaluation criterion that covers these region-differentiated goals is desired. Meanwhile, the SR is performed generally for better human visual perception. Therefore, how to develop an automatic model that can measure visual quality more accurately and conveniently remains a challenge. Furthermore, there are no HR images for reference in practical applications. Thus the no-reference quality assessment criteria for super-resolved images have great demands.

VII. CONCLUSION

In recent years the super-resolution of real-world images has been getting increased attention. This paper briefly reviews recent super-resolution methods for realistic images, including degradation modeling-based algorithms, image pairs-based algorithms, domain translation-based algorithms, and self-learning-based algorithms. Meanwhile, we summarize the commonly used datasets and assessment metrics for RSISR models training and evaluation. Moreover, although some progress has been made on RSISR in the past few years, we point out that there are still challenges to be further addressed, *e.g.*, realistic datasets for model training and testing, specific models for real-world image super-resolution and reconstruction performance evaluation. These unsolved problems also indicate the promising directions for future exploration. We expect that this review can give a better understanding of existing studies for researchers, and also hope that it can attract more attention to advance the progress and application of real-world image super-resolution techniques.

REFERENCES

- [1] D. Dai, Y. Wang, Y. Chen, and L. Van Gool, "Is image super-resolution helpful for other vision tasks?" in *IEEE Winter Conference on Applications of Computer Vision (WACV)*, 2016, pp. 1–9.
- [2] S. Lei, Z. Shi, X. Wu, B. Pan, X. Xu, and H. Hao, "Simultaneous super-resolution and segmentation for remote sensing images," in *IEEE International Geoscience and Remote Sensing Symposium (IGARSS)*, 2019, pp. 3121–3124.
- [3] Z. Guo, G. Wu, X. Song, W. Yuan, Q. Chen, H. Zhang, X. Shi, M. Xu, Y. Xu, R. Shibasaki *et al.*, "Super-resolution integrated building semantic segmentation for multi-source remote sensing imagery," *IEEE Access*, vol. 7, pp. 99 381–99 397, 2019.
- [4] L. Wang, D. Li, Y. Zhu, L. Tian, and Y. Shan, "Dual super-resolution learning for semantic segmentation," in *Proceedings of the IEEE Conference on Computer Vision and Pattern Recognition (CVPR)*, 2020, pp. 3774–3783.
- [5] M. Haris, G. Shakhnarovich, and N. Ukita, "Task-driven super resolution: Object detection in low-resolution images," *arXiv preprint arXiv:1803.11316*, 2018.
- [6] Y. Pang, J. Cao, J. Wang, and J. Han, "JCS-Net: Joint classification and super-resolution network for small-scale pedestrian detection in surveillance images," *IEEE Transactions on Information Forensics and Security*, vol. 14, no. 12, pp. 3322–3331, 2019.
- [7] Y. Zhang, Y. Bai, M. Ding, S. Xu, and B. Ghanem, "KGSnet: key-point-guided super-resolution network for pedestrian detection in the wild," *IEEE Transactions on Neural Networks and Learning Systems*, 2020.
- [8] Z. Wang, S. Chang, Y. Yang, D. Liu, and T. S. Huang, "Studying very low resolution recognition using deep networks," in *Proceedings of the IEEE Conference on Computer Vision and Pattern Recognition (CVPR)*, 2016, pp. 4792–4800.
- [9] X. Yang, W. Wu, K. Liu, P. W. Kim, A. K. Sangaiah, and G. Jeon, "Long-distance object recognition with image super resolution: A comparative study," *IEEE Access*, vol. 6, pp. 13 429–13 438, 2018.
- [10] T. Suprpto Siadari, M. Han, and H. Yoon, "GSR-MAR: Global super-resolution for person multi-attribute recognition," in *Proceedings of the IEEE International Conference on Computer Vision Workshops (ICCVW)*, 2019.
- [11] S. P. Belekos, N. P. Galatsanos, and A. K. Katsaggelos, "Maximum a posteriori video super-resolution using a new multichannel image prior," *IEEE Transactions on Image Processing*, vol. 19, no. 6, pp. 1451–1464, 2010.
- [12] C. Liu and D. Sun, "On bayesian adaptive video super resolution," *IEEE Transactions on Pattern Analysis and Machine Intelligence*, vol. 36, no. 2, pp. 346–360, 2013.
- [13] K. Li, Y. Zhu, J. Yang, and J. Jiang, "Video super-resolution using an adaptive superpixel-guided auto-regressive model," *Pattern Recognition*, vol. 51, pp. 59–71, 2016.
- [14] A. Kappeler, S. Yoo, Q. Dai, and A. K. Katsaggelos, "Video super-resolution with convolutional neural networks," *IEEE Transactions on Computational Imaging*, vol. 2, no. 2, pp. 109–122, 2016.
- [15] J. Caballero, C. Ledig, A. Aitken, A. Acosta, J. Totz, Z. Wang, and W. Shi, "Real-time video super-resolution with spatio-temporal networks and motion compensation," in *Proceedings of the IEEE Conference on Computer Vision and Pattern Recognition (CVPR)*, 2017, pp. 4778–4787.
- [16] Y. Jo, S. Wug Oh, J. Kang, and S. Joo Kim, "Deep video super-resolution network using dynamic upsampling filters without explicit motion compensation," in *Proceedings of the IEEE conference on Computer Vision and Pattern Recognition (CVPR)*, 2018, pp. 3224–3232.
- [17] A. Lucas, S. Lopez-Tapia, R. Molina, and A. K. Katsaggelos, "Generative adversarial networks and perceptual losses for video super-resolution," *IEEE Transactions on Image Processing*, vol. 28, no. 7, pp. 3312–3327, 2019.
- [18] M. Haris, G. Shakhnarovich, and N. Ukita, "Recurrent back-projection network for video super-resolution," in *Proceedings of the IEEE Conference on Computer Vision and Pattern Recognition (CVPR)*, 2019, pp. 3897–3906.
- [19] Y. Tian, Y. Zhang, Y. Fu, and C. Xu, "TDAN: Temporally-deformable alignment network for video super-resolution," in *Proceedings of the IEEE Conference on Computer Vision and Pattern Recognition (CVPR)*, 2020, pp. 3360–3369.
- [20] S. Dikbas and Y. Altunbasak, "Novel true-motion estimation algorithm and its application to motion-compensated temporal frame interpolation," *IEEE Transactions on Image Processing*, vol. 22, no. 8, pp. 2931–2945, 2012.
- [21] B.-D. Choi, J.-W. Han, C.-S. Kim, and S.-J. Ko, "Motion-compensated frame interpolation using bilateral motion estimation and adaptive overlapped block motion compensation," *IEEE Transactions on Circuits and Systems for Video Technology*, vol. 17, no. 4, pp. 407–416, 2007.
- [22] S. Niklaus, L. Mai, and F. Liu, "Video frame interpolation via adaptive separable convolution," in *Proceedings of the IEEE International Conference on Computer Vision (ICCV)*, 2017, pp. 261–270.
- [23] S. Niklaus and F. Liu, "Context-aware synthesis for video frame interpolation," in *Proceedings of the IEEE Conference on Computer Vision and Pattern Recognition (CVPR)*, 2018, pp. 1701–1710.
- [24] W. Bao, W.-S. Lai, C. Ma, X. Zhang, Z. Gao, and M.-H. Yang, "Depth-aware video frame interpolation," in *Proceedings of the IEEE Conference on Computer Vision and Pattern Recognition (CVPR)*, 2019, pp. 3703–3712.
- [25] T. Peleg, P. Szekeley, D. Sabo, and O. Sendik, "IM-Net for high resolution video frame interpolation," in *Proceedings of the IEEE Conference on Computer Vision and Pattern Recognition (CVPR)*, 2019, pp. 2398–2407.
- [26] W. Bao, W.-S. Lai, X. Zhang, Z. Gao, and M.-H. Yang, "MEMC-Net: Motion estimation and motion compensation driven neural network for video interpolation and enhancement," *IEEE Transactions on Pattern Analysis and Machine Intelligence*, 2019.
- [27] X. Cheng and Z. Chen, "Video frame interpolation via deformable separable convolution," in *AAAI*, 2020, pp. 10 607–10 614.

- [28] S. Farsiu, M. D. Robinson, M. Elad, and P. Milanfar, "Fast and robust multiframe super resolution," *IEEE Transactions on Image Processing*, vol. 13, no. 10, pp. 1327–1344, 2004.
- [29] S. Farsiu, M. Elad, and P. Milanfar, "Multiframe demosaicing and super-resolution of color images," *IEEE Transactions on Image Processing*, vol. 15, no. 1, pp. 141–159, 2005.
- [30] X. Li, Y. Hu, X. Gao, D. Tao, and B. Ning, "A multi-frame image super-resolution method," *Signal Processing*, vol. 90, no. 2, pp. 405–414, 2010.
- [31] Q. Yuan, L. Zhang, and H. Shen, "Multiframe super-resolution employing a spatially weighted total variation model," *IEEE Transactions on Circuits and Systems for Video Technology*, vol. 22, no. 3, pp. 379–392, 2011.
- [32] L. Yue, H. Shen, Q. Yuan, and L. Zhang, "A locally adaptive 11- 12 norm for multi-frame super-resolution of images with mixed noise and outliers," *Signal Processing*, vol. 105, pp. 156–174, 2014.
- [33] T. Köhler, X. Huang, F. Schebesch, A. Aichert, A. Maier, and J. Hornegger, "Robust multiframe super-resolution employing iteratively re-weighted minimization," *IEEE Transactions on Computational Imaging*, vol. 2, no. 1, pp. 42–58, 2016.
- [34] X. Liu, L. Chen, W. Wang, and J. Zhao, "Robust multi-frame super-resolution based on spatially weighted half-quadratic estimation and adaptive btv regularization," *IEEE Transactions on Image Processing*, vol. 27, no. 10, pp. 4971–4986, 2018.
- [35] A. Laghrib, A. Hadri, A. Hakim, and S. Raghay, "A new multiframe super-resolution based on nonlinear registration and a spatially weighted regularization," *Information Sciences*, vol. 493, pp. 34–56, 2019.
- [36] J. Sun, Z. Xu, and H.-Y. Shum, "Image super-resolution using gradient profile prior," in *IEEE Conference on Computer Vision and Pattern Recognition (CVPR)*, 2008, pp. 1–8.
- [37] K. Zhang, X. Gao, D. Tao, and X. Li, "Single image super-resolution with non-local means and steering kernel regression," *IEEE Transactions on Image Processing*, vol. 21, no. 11, pp. 4544–4556, 2012.
- [38] W. Dong, L. Zhang, G. Shi, and X. Li, "Nonlocally centralized sparse representation for image restoration," *IEEE Transactions on Image Processing*, vol. 22, no. 4, pp. 1620–1630, 2013.
- [39] V. Pappyan and M. Elad, "Multi-scale patch-based image restoration," *IEEE Transactions on Image Processing*, vol. 25, no. 1, pp. 249–261, 2015.
- [40] J. Jiang, X. Ma, C. Chen, T. Lu, Z. Wang, and J. Ma, "Single image super-resolution via locally regularized anchored neighborhood regression and nonlocal means," *IEEE Transactions on Multimedia*, vol. 19, no. 1, pp. 15–26, 2017.
- [41] C. Ren, X. He, and T. Q. Nguyen, "Single image super-resolution via adaptive high-dimensional non-local total variation and adaptive geometric feature," *IEEE Transactions on Image Processing*, vol. 26, no. 1, pp. 90–106, 2017.
- [42] H. Chen, X. He, L. Qing, and Q. Teng, "Single image super-resolution via adaptive transform-based nonlocal self-similarity modeling and learning-based gradient regularization," *IEEE Transactions on Multimedia*, vol. 19, no. 8, pp. 1702–1717, 2017.
- [43] K. Chang, X. Zhang, P. L. K. Ding, and B. Li, "Data-adaptive low-rank modeling and external gradient prior for single image super-resolution," *Signal Processing*, vol. 161, pp. 36–49, 2019.
- [44] T. Li, X. Dong, and H. Chen, "Single image super-resolution incorporating example-based gradient profile estimation and weighted adaptive p-norm," *Neurocomputing*, vol. 355, pp. 105–120, 2019.
- [45] J. Li and W. Guan, "Adaptive l_q -norm constrained general nonlocal self-similarity regularizer based sparse representation for single image super-resolution," *Information Fusion*, vol. 53, pp. 88–102, 2020.
- [46] W. T. Freeman, T. R. Jones, and E. C. Pasztor, "Example-based super-resolution," *IEEE Computer Graphics and Applications*, vol. 22, no. 2, pp. 56–65, 2002.
- [47] D. Glasner, S. Bagon, and M. Irani, "Super-resolution from a single image," in *IEEE International Conference on Computer Vision (ICCV)*, 2009, pp. 349–356.
- [48] Z. Xiong, D. Xu, X. Sun, and F. Wu, "Example-based super-resolution with soft information and decision," *IEEE Transactions on Multimedia*, vol. 15, no. 6, pp. 1458–1465, 2013.
- [49] Y. Zhu, Y. Zhang, and A. L. Yuille, "Single image super-resolution using deformable patches," in *Proceedings of the IEEE Conference on Computer Vision and Pattern Recognition (CVPR)*, 2014, pp. 2917–2924.
- [50] J.-B. Huang, A. Singh, and N. Ahuja, "Single image super-resolution from transformed self-exemplars," in *Proceedings of the IEEE Conference on Computer Vision and Pattern Recognition (CVPR)*, 2015, pp. 5197–5206.
- [51] T. Li, X. He, Q. Teng, and X. Wu, "Rotation expanded dictionary-based single image super-resolution," *Neurocomputing*, vol. 216, pp. 1–17, 2016.
- [52] J.-J. Huang, T. Liu, P. Luigi Dragotti, and T. Stathaki, "SRHRF+: Self-example enhanced single image super-resolution using hierarchical random forests," in *Proceedings of the IEEE Conference on Computer Vision and Pattern Recognition Workshops (CVPRW)*, 2017, pp. 71–79.
- [53] J. Yang, J. Wright, T. S. Huang, and Y. Ma, "Image super-resolution via sparse representation," *IEEE Transactions on Image Processing*, vol. 19, no. 11, pp. 2861–2873, 2010.
- [54] R. Zeyde, M. Elad, and M. Protter, "On single image scale-up using sparse-representations," in *International Conference on Curves and Surfaces*, 2010, pp. 711–730.
- [55] S. Wang, L. Zhang, Y. Liang, and Q. Pan, "Semi-coupled dictionary learning with applications to image super-resolution and photo-sketch synthesis," in *IEEE Conference on Computer Vision and Pattern Recognition (CVPR)*, 2012, pp. 2216–2223.
- [56] Z. Zhu, F. Guo, H. Yu, and C. Chen, "Fast single image super-resolution via self-example learning and sparse representation," *IEEE Transactions on Multimedia*, vol. 16, no. 8, pp. 2178–2190, 2014.
- [57] L.-W. Kang, C.-C. Hsu, B. Zhuang, C.-W. Lin, and C.-H. Yeh, "Learning-based joint super-resolution and deblocking for a highly compressed image," *IEEE Transactions on Multimedia*, vol. 17, no. 7, pp. 921–934, 2015.
- [58] X. Li, G. Cao, Y. Zhang, A. Shafique, and P. Fu, "Combining synthesis sparse with analysis sparse for single image super-resolution," *Signal Processing: Image Communication*, vol. 83, p. 115805, 2020.
- [59] B. Li, Y. Zhou, Y. Zhang, and A. Wang, "Depth image super-resolution based on joint sparse coding," *Pattern Recognition Letters*, vol. 130, pp. 21–29, 2020.
- [60] S. Ayas and M. Ekinici, "Single image super resolution using dictionary learning and sparse coding with multi-scale and multi-directional gabor feature representation," *Information Sciences*, vol. 512, pp. 1264–1278, 2020.
- [61] R. Timofte, V. De Smet, and L. Van Gool, "Anchored neighborhood regression for fast example-based super-resolution," in *Proceedings of the IEEE International Conference on Computer Vision (ICCV)*, 2013, pp. 1920–1927.
- [62] —, "A+: Adjusted anchored neighborhood regression for fast super-resolution," in *Asian Conference on Computer Vision (ACCV)*, 2014, pp. 111–126.
- [63] K. Zhang, B. Wang, W. Zuo, H. Zhang, and L. Zhang, "Joint learning of multiple regressors for single image super-resolution," *IEEE Signal Processing Letters*, vol. 23, no. 1, pp. 102–106, 2015.
- [64] E. Agustsson, R. Timofte, and L. Van Gool, "Regressor basis learning for anchored super-resolution," in *2016 23rd International Conference on Pattern Recognition (ICPR)*, 2016, pp. 3850–3855.
- [65] E. Perez-Pellitero, J. Salvador, J. Ruiz-Hidalgo, and B. Rosenhahn, "Antipodally invariant metrics for fast regression-based super-resolution," *IEEE Transactions on Image Processing*, vol. 25, no. 6, pp. 2456–2468, 2016.
- [66] K. Zhang, Z. Wang, J. Li, X. Gao, and Z. Xiong, "Learning recurrent residual regressors for single image super-resolution," *Signal Processing*, vol. 154, pp. 324–337, 2019.
- [67] C. Dong, C. C. Loy, K. He, and X. Tang, "Image super-resolution using deep convolutional networks," *IEEE Transactions on Pattern Analysis and Machine Intelligence*, vol. 38, no. 2, pp. 295–307, 2015.
- [68] J. Kim, J. Kwon Lee, and K. Mu Lee, "Accurate image super-resolution using very deep convolutional networks," in *Proceedings of the IEEE Conference on Computer Vision and Pattern Recognition (CVPR)*, 2016, pp. 1646–1654.
- [69] C. Ledig, L. Theis, F. Huszár, J. Caballero, A. Cunningham, A. Acosta, A. Aitken, A. Tejani, J. Totz, Z. Wang *et al.*, "Photo-realistic single image super-resolution using a generative adversarial network," in *Proceedings of the IEEE Conference on Computer Vision and Pattern Recognition (CVPR)*, 2017, pp. 4681–4690.
- [70] B. Lim, S. Son, H. Kim, S. Nah, and K. Mu Lee, "Enhanced deep residual networks for single image super-resolution," in *Proceedings of the IEEE Conference on Computer Vision and Pattern Recognition Workshops (CVPRW)*, 2017, pp. 136–144.
- [71] M. Haris, G. Shakhnarovich, and N. Ukita, "Deep back-projection networks for super-resolution," in *Proceedings of the IEEE Conference on Computer Vision and Pattern Recognition (CVPR)*, 2018, pp. 1664–1673.

- [72] W.-S. Lai, J.-B. Huang, N. Ahuja, and M.-H. Yang, "Fast and accurate image super-resolution with deep laplacian pyramid networks," *IEEE Transactions on Pattern Analysis and Machine Intelligence*, vol. 41, no. 11, pp. 2599–2613, 2018.
- [73] Y. Zhang, K. Li, K. Li, L. Wang, B. Zhong, and Y. Fu, "Image super-resolution using very deep residual channel attention networks," in *Proceedings of the European Conference on Computer Vision (ECCV)*, 2018, pp. 286–301.
- [74] Y. Zhang, Y. Tian, Y. Kong, B. Zhong, and Y. Fu, "Residual dense network for image super-resolution," in *Proceedings of the IEEE Conference on Computer Vision and Pattern Recognition (CVPR)*, 2018, pp. 2472–2481.
- [75] T. Dai, J. Cai, Y. Zhang, S.-T. Xia, and L. Zhang, "Second-order attention network for single image super-resolution," in *Proceedings of the IEEE Conference on Computer Vision and Pattern Recognition (CVPR)*, 2019, pp. 11 065–11 074.
- [76] Y. Guo, J. Chen, J. Wang, Q. Chen, J. Cao, Z. Deng, Y. Xu, and M. Tan, "Closed-loop matters: Dual regression networks for single image super-resolution," in *Proceedings of the IEEE Conference on Computer Vision and Pattern Recognition (CVPR)*, 2020, pp. 5407–5416.
- [77] J. Liu, W. Zhang, Y. Tang, J. Tang, and G. Wu, "Residual feature aggregation network for image super-resolution," in *Proceedings of the IEEE Conference on Computer Vision and Pattern Recognition (CVPR)*, 2020.
- [78] X. Zhang, H. Dong, Z. Hu, W.-S. Lai, F. Wang, and M.-H. Yang, "Gated fusion network for degraded image super resolution," *International Journal of Computer Vision*, pp. 1–23, 2020.
- [79] T. Köhler, M. Bätz, F. Naderi, A. Kaup, A. Maier, and C. Riess, "Toward bridging the simulated-to-real gap: Benchmarking super-resolution on real data," *IEEE Transactions on Pattern Analysis and Machine Intelligence*, vol. 42, no. 11, pp. 2944–2959, 2020.
- [80] J. Cai, H. Zeng, H. Yong, Z. Cao, and L. Zhang, "Toward real-world single image super-resolution: A new benchmark and a new model," in *Proceedings of the IEEE International Conference on Computer Vision (ICCV)*, 2019, pp. 3086–3095.
- [81] P. Wei, Z. Xie, H. Lu, Z. Zhan, Q. Ye, W. Zuo, and L. Lin, "Component divide-and-conquer for real-world image super-resolution," in *European Conference on Computer Vision (ECCV)*, 2020.
- [82] C. Chen, Z. Xiong, X. Tian, Z.-J. Zha, and F. Wu, "Camera lens super-resolution," in *Proceedings of the IEEE Conference on Computer Vision and Pattern Recognition (CVPR)*, 2019, pp. 1652–1660.
- [83] X. Zhang, Q. Chen, R. Ng, and V. Koltun, "Zoom to learn, learn to zoom," in *Proceedings of the IEEE Conference on Computer Vision and Pattern Recognition (CVPR)*, 2019, pp. 3762–3770.
- [84] W. Wang, E. Xie, X. Liu, W. Wang, D. Liang, C. Shen, and X. Bai, "Scene text image super-resolution in the wild," in *European Conference on Computer Vision (ECCV)*, 2020.
- [85] H. Reza Vaezi Joze, I. Zharkov, K. Powell, C. Ringler, L. Liang, A. Roulston, M. Lutz, and V. Pradeep, "ImagePairs: Realistic super resolution dataset via beam splitter camera rig," in *Proceedings of the IEEE Conference on Computer Vision and Pattern Recognition Workshops (CVPRW)*, 2020, pp. 518–519.
- [86] X. Xu, Y. Ma, and W. Sun, "Towards real scene super-resolution with raw images," in *Proceedings of the IEEE Conference on Computer Vision and Pattern Recognition (CVPR)*, 2019, pp. 1723–1731.
- [87] X. Xu, Y. Ma, W. Sun, and M.-H. Yang, "Exploiting raw images for real-scene super-resolution," *IEEE Transactions on Pattern Analysis and Machine Intelligence*, 2020.
- [88] W.-Z. Shao and M. Elad, "Simple, accurate, and robust nonparametric blind super-resolution," in *International Conference on Image and Graphics (ICIG)*, 2015, pp. 333–348.
- [89] W.-Z. Shao, Q. Ge, L.-Q. Wang, Y.-Z. Lin, H.-S. Deng, and H.-B. Li, "Nonparametric blind super-resolution using adaptive heavy-tailed priors," *Journal of Mathematical Imaging and Vision*, vol. 61, no. 6, pp. 885–917, 2019.
- [90] J. Gu, H. Lu, W. Zuo, and C. Dong, "Blind super-resolution with iterative kernel correction," in *Proceedings of the IEEE Conference on Computer Vision and Pattern Recognition (CVPR)*, 2019, pp. 1604–1613.
- [91] V. Cornillere, A. Djelouah, W. Yifan, O. Sorkine-Hornung, and C. Schroers, "Blind image super-resolution with spatially variant degradations," *ACM Transactions on Graphics*, vol. 38, no. 6, pp. 1–13, 2019.
- [92] Y. Huang, S. Li, L. Wang, T. Tan *et al.*, "Unfolding the alternating optimization for blind super resolution," in *34th Conference on Neural Information Processing Systems (NeurIPS)*, 2020.
- [93] T. Michaeli and M. Irani, "Nonparametric blind super-resolution," in *Proceedings of the IEEE International Conference on Computer Vision (ICCV)*, 2013, pp. 945–952.
- [94] S. Bell-Kligler, A. Shocher, and M. Irani, "Blind super-resolution kernel estimation using an internal-gan," in *33rd Conference on Neural Information Processing Systems (NeurIPS)*, 2019, pp. 284–293.
- [95] A. Bulat, J. Yang, and G. Tzimiropoulos, "To learn image super-resolution, use a gan to learn how to do image degradation first," in *Proceedings of the European Conference on Computer Vision (ECCV)*, 2018, pp. 185–200.
- [96] R. Zhou and S. Susstrunk, "Kernel modeling super-resolution on real low-resolution images," in *Proceedings of the IEEE International Conference on Computer Vision (ICCV)*, 2019, pp. 2433–2443.
- [97] J. Xiao, H. Yong, and L. Zhang, "Degradation model learning for real-world single image super-resolution," in *Proceedings of the Asian Conference on Computer Vision (ACCV)*, 2020.
- [98] X. Ji, Y. Cao, Y. Tai, C. Wang, J. Li, and F. Huang, "Real-world super-resolution via kernel estimation and noise injection," in *Proceedings of the IEEE Conference on Computer Vision and Pattern Recognition Workshops (CVPRW)*, 2020, pp. 466–467.
- [99] Y. Yuan, S. Liu, J. Zhang, Y. Zhang, C. Dong, and L. Lin, "Unsupervised image super-resolution using cycle-in-cycle generative adversarial networks," in *Proceedings of the IEEE Conference on Computer Vision and Pattern Recognition Workshops (CVPRW)*, 2018, pp. 701–710.
- [100] Y. Zhang, S. Liu, C. Dong, X. Zhang, and Y. Yuan, "Multiple cycle-in-cycle generative adversarial networks for unsupervised image super-resolution," *IEEE Transactions on Image Processing*, vol. 29, pp. 1101–1112, 2020.
- [101] G. Kim, J. Park, K. Lee, J. Lee, J. Min, B. Lee, D. K. Han, and H. Ko, "Unsupervised real-world super resolution with cycle generative adversarial network and domain discriminator," in *Proceedings of the IEEE Conference on Computer Vision and Pattern Recognition Workshops (CVPRW)*, 2020, pp. 456–457.
- [102] S. Maeda, "Unpaired image super-resolution using pseudo-supervision," in *Proceedings of the IEEE Conference on Computer Vision and Pattern Recognition (CVPR)*, 2020, pp. 291–300.
- [103] K. Prajapati, V. Chudasama, H. Patel, K. Upla, R. Ramachandra, K. Raja, and C. Busch, "Unsupervised single image super-resolution network (USISResNet) for real-world data using generative adversarial network," in *Proceedings of the IEEE Conference on Computer Vision and Pattern Recognition Workshops (CVPRW)*, 2020, pp. 464–465.
- [104] T. Zhao, W. Ren, C. Zhang, D. Ren, and Q. Hu, "Unsupervised degradation learning for single image super-resolution," *arXiv preprint arXiv:1812.04240*, 2018.
- [105] C. You, G. Li, Y. Zhang, X. Zhang, H. Shan, M. Li, S. Ju, Z. Zhao, Z. Zhang, W. Cong *et al.*, "CT super-resolution gan constrained by the identical, residual, and cycle learning ensemble (GAN-CIRCLE)," *IEEE Transactions on Medical Imaging*, vol. 39, no. 1, pp. 188–203, 2020.
- [106] M. Fritsche, S. Gu, and R. Timofte, "Frequency separation for real-world super-resolution," in *IEEE International Conference on Computer Vision Workshop (ICCVW)*, 2019, pp. 3599–3608.
- [107] R. Muhammad Umer, G. Luca Foresti, and C. Micheloni, "Deep generative adversarial residual convolutional networks for real-world super-resolution," in *Proceedings of the IEEE Conference on Computer Vision and Pattern Recognition Workshops (CVPRW)*, 2020, pp. 438–439.
- [108] M. S. Rad, T. Yu, C. Musat, H. K. Ekenel, B. Bozorgtabar, and J.-P. Thiran, "Benefiting from bicubically down-sampled images for learning real-world image super-resolution," in *Proceedings of the IEEE Winter Conference on Applications of Computer Vision (WACV)*, 2021, pp. 1590–1599.
- [109] A. Lugmayr, M. Danelljan, and R. Timofte, "Unsupervised learning for real-world super-resolution," in *IEEE International Conference on Computer Vision Workshop (ICCVW)*, 2019, pp. 3408–3416.
- [110] S. Chen, Z. Han, E. Dai, X. Jia, Z. Liu, L. Xing, X. Zou, C. Xu, J. Liu, and Q. Tian, "Unsupervised image super-resolution with an indirect supervised path," in *Proceedings of the IEEE Conference on Computer Vision and Pattern Recognition Workshops (CVPRW)*, 2020, pp. 468–469.
- [111] A. Shocher, N. Cohen, and M. Irani, "'Zero-Shot' super-resolution using deep internal learning," in *Proceedings of the IEEE Conference on Computer Vision and Pattern Recognition (CVPR)*, 2018, pp. 3118–3126.

- [112] J. Kim, C. Jung, and C. Kim, "Dual back-projection-based internal learning for blind super-resolution," *IEEE Signal Processing Letters*, vol. 27, pp. 1190–1194, 2020.
- [113] M. Emad, M. Peemen, and H. Corporaal, "DualSR: Zero-shot dual learning for real-world super-resolution," in *Proceedings of the IEEE Winter Conference on Applications of Computer Vision (WACV)*, 2021, pp. 1630–1639.
- [114] J. W. Soh, S. Cho, and N. I. Cho, "Meta-transfer learning for zero-shot super-resolution," in *Proceedings of the IEEE Conference on Computer Vision and Pattern Recognition (CVPR)*, 2020, pp. 3516–3525.
- [115] S. Park, J. Yoo, D. Cho, J. Kim, and T. H. Kim, "Fast adaptation to super-resolution networks via meta-learning," in *European Conference on Computer Vision (ECCV)*, 2020.
- [116] C. Ma, C.-Y. Yang, X. Yang, and M.-H. Yang, "Learning a no-reference quality metric for single-image super-resolution," *Computer Vision and Image Understanding*, vol. 158, pp. 1–16, 2017.
- [117] Y. Fang, C. Zhang, W. Yang, J. Liu, and Z. Guo, "Blind visual quality assessment for image super-resolution by convolutional neural network," *Multimedia Tools and Applications*, vol. 77, no. 22, pp. 29 829–29 846, 2018.
- [118] B. Bare, K. Li, B. Yan, B. Feng, and C. Yao, "A deep learning based no-reference image quality assessment model for single-image super-resolution," in *2018 IEEE International Conference on Acoustics, Speech and Signal Processing (ICASSP)*. IEEE, 2018, pp. 1223–1227.
- [119] M. Greeshma and V. Bindu, "Super-resolution quality criterion (srqc): a super-resolution image quality assessment metric," *Multimedia Tools and Applications*, pp. 1–22, 2020.
- [120] J. Cai, S. Gu, R. Timofte, and L. Zhang, "NTIRE 2019 challenge on real image super-resolution: Methods and results," in *Proceedings of the IEEE Conference on Computer Vision and Pattern Recognition Workshops (CVPRW)*, 2019, pp. 2211–2223.
- [121] A. Lugmayr, M. Danelljan, R. Timofte, M. Fritsche, S. Gu, K. Purohit, P. Kandula, M. Suin, A. Rajagoopalan, N. H. Joon *et al.*, "AIM 2019 challenge on real-world image super-resolution: Methods and results," in *IEEE International Conference on Computer Vision Workshop (ICCVW)*, 2019, pp. 3575–3583.
- [122] A. Lugmayr, M. Danelljan, and R. Timofte, "NTIRE 2020 challenge on real-world image super-resolution: Methods and results," in *Proceedings of the IEEE Conference on Computer Vision and Pattern Recognition Workshops (CVPRW)*, 2020, pp. 494–495.
- [123] P. Wei, H. Lu, R. Timofte, L. Lin, W. Zuo, Z. Pan, B. Li, T. Xi, Y. Fan, G. Zhang *et al.*, "AIM 2020 challenge on real image super-resolution: Methods and results," in *European Conference on Computer Vision Workshops (ECCVW)*, 2020.
- [124] L. Yue, H. Shen, J. Li, Q. Yuan, H. Zhang, and L. Zhang, "Image super-resolution: The techniques, applications, and future," *Signal Processing*, vol. 128, pp. 389–408, 2016.
- [125] W. Yang, X. Zhang, Y. Tian, W. Wang, J.-H. Xue, and Q. Liao, "Deep learning for single image super-resolution: A brief review," *IEEE Transactions on Multimedia*, vol. 21, no. 12, pp. 3106–3121, 2019.
- [126] Z. Wang, J. Chen, and S. C. Hoi, "Deep learning for image super-resolution: A survey," *IEEE Transactions on Pattern Analysis and Machine Intelligence*, 2020.
- [127] H. Liu, Z. Ruan, P. Zhao, F. Shang, L. Yang, and Y. Liu, "Video super resolution based on deep learning: A comprehensive survey," *arXiv preprint arXiv:2007.12928*, 2020.
- [128] E. Agustsson and R. Timofte, "NTIRE 2017 challenge on single image super-resolution: Dataset and study," in *Proceedings of the IEEE Conference on Computer Vision and Pattern Recognition Workshops (CVPRW)*, 2017, pp. 126–135.
- [129] P. Arbelaez, M. Maire, C. Fowlkes, and J. Malik, "Contour detection and hierarchical image segmentation," *IEEE Transactions on Pattern Analysis and Machine Intelligence*, vol. 33, no. 5, pp. 898–916, 2011.
- [130] M. Bevilacqua, A. Roumy, C. Guillemot, and M.-L. A. Morel, "Low-complexity single-image super-resolution based on nonnegative neighbor embedding," in *British Machine Vision Conference (BMVC)*, 2012.
- [131] A. Fujimoto, T. Ogawa, K. Yamamoto, Y. Matsui, T. Yamasaki, and K. Aizawa, "Manga109 dataset and creation of metadata," in *Proceedings of the 1st International Workshop on Comics Analysis, Processing and Understanding*, 2016, pp. 1–5.
- [132] D. G. Lowe, "Distinctive image features from scale-invariant keypoints," *International Journal of Computer Vision*, vol. 60, no. 2, pp. 91–110, 2004.
- [133] M. A. Fischler and R. C. Bolles, "Random sample consensus: a paradigm for model fitting with applications to image analysis and automated cartography," *Communications of the ACM*, vol. 24, no. 6, pp. 381–395, 1981.
- [134] G. D. Evangelidis and E. Z. Psarakis, "Parametric image alignment using enhanced correlation coefficient maximization," *IEEE Transactions on Pattern Analysis and Machine Intelligence*, vol. 30, no. 10, pp. 1858–1865, 2008.
- [135] Z. Wang, A. C. Bovik, H. R. Sheikh, and E. P. Simoncelli, "Image quality assessment: from error visibility to structural similarity," *IEEE Transactions on Image Processing*, vol. 13, no. 4, pp. 600–612, 2004.
- [136] H. R. Sheikh, A. C. Bovik, and G. De Veciana, "An information fidelity criterion for image quality assessment using natural scene statistics," *IEEE Transactions on Image Processing*, vol. 14, no. 12, pp. 2117–2128, 2005.
- [137] R. Zhang, P. Isola, A. A. Efros, E. Shechtman, and O. Wang, "The unreasonable effectiveness of deep features as a perceptual metric," in *Proceedings of the IEEE Conference on Computer Vision and Pattern Recognition (CVPR)*, 2018, pp. 586–595.
- [138] A. Mittal, R. Soundararajan, and A. C. Bovik, "Making a 'completely blind' image quality analyzer," *IEEE Signal Processing Letters*, vol. 20, no. 3, pp. 209–212, 2012.
- [139] N. Venkatanath, D. Praneeth, M. C. Bh, S. S. Channappayya, and S. S. Medasani, "Blind image quality evaluation using perception based features," in *2015 Twenty First National Conference on Communications (NCC)*, 2015, pp. 1–6.
- [140] C.-Y. Yang, C. Ma, and M.-H. Yang, "Single-image super-resolution: A benchmark," in *European Conference on Computer Vision (ECCV)*, 2014, pp. 372–386.
- [141] N. Efraz, D. Glasner, A. Apartsin, B. Nadler, and A. Levin, "Accurate blur models vs. image priors in single image super-resolution," in *Proceedings of the IEEE International Conference on Computer Vision (ICCV)*, 2013, pp. 2832–2839.
- [142] R. Mechrez, I. Talmi, and L. Zelnik-Manor, "The contextual loss for image transformation with non-aligned data," in *Proceedings of the European Conference on Computer Vision (ECCV)*, 2018, pp. 768–783.
- [143] C. Tomasi and R. Manduchi, "Bilateral filtering for gray and color images," in *IEEE International Conference on Computer Vision (ICCV)*, 1998, pp. 839–846.
- [144] K. Simonyan and A. Zisserman, "Very deep convolutional networks for large-scale image recognition," in *International Conference on Learning Representations (ICLR)*, 2015.
- [145] J.-Y. Zhu, T. Park, P. Isola, and A. A. Efros, "Unpaired image-to-image translation using cycle-consistent adversarial networks," in *Proceedings of the IEEE International Conference on Computer Vision (ICCV)*, 2017, pp. 2223–2232.
- [146] X. Wang, K. Yu, S. Wu, J. Gu, Y. Liu, C. Dong, Y. Qiao, and C. Change Loy, "ESRGAN: Enhanced super-resolution generative adversarial networks," in *Proceedings of the European Conference on Computer Vision Workshops (ECCVW)*, 2018.
- [147] C. Finn, P. Abbeel, and S. Levine, "Model-agnostic meta-learning for fast adaptation of deep networks," in *International Conference on Machine Learning (ICML)*, 2017.